S&G3640

ATTENUATION OF WEAK GROUND MOTIONS

Aasha Pancha and J. John Taber

School of Earth Sciences
Victoria University of Wellington

A Report prepared for
the New Zealand Earthquake Commission

August 1997

Contents

Non-technical Summary

Attenuation relations using weak ground motion recordings have been determined using data from the New Zealand National Seismograph Network and several temporary seismograph deployments. Models have been developed for earthquake sources in four regions: Eastern North Island Shallow, Eastern North Island Deep, Central Volcanic Region Shallow and the Central Volcanic Region Deep. Earthquakes were classified as deep if they occurred below 33 km. Equations have been fit to the data for each of the regions using two different attenuation models.

Attenuation rates were found to be greatest in the shallow Central Volcanic Region. Eastern North Island Deep attenuation rates were similar to Eastern North Island Shallow rates. The lowest attenuation rate was found for earthquakes within the Central Volcanic Deep Region that were recorded in the Eastern North Island. This is consistent with a low rate of attenuation in the subducting Pacific plate.

Although the measured attenuation rate is comparable to some strong-motion relations, the absolute level of strong-motion attenuation curves greatly differs from those of the weak-motion, particularly at low magnitudes. This may be due to a number of factors. Unlike models within the literature which used near-field strong-motion data, far-field weak-motion data has been used for this study. A second possible explanation for the difference in absolute level is a change in frequency characteristics between large and small earthquakes. Most importantly, differences may result from the use of different magnitude scales in the weak-motion and strong-motion models. The magnitude scale difference appears to be the primary reason for the difference in absolute level between the weak-motion and strong-motion relations. This implies that while some terms in the derived attenuation equations are different from strong-motion models, the attenuation rate term should be comparable.

A variation of peak ground acceleration with changes in direction of travel of the seismic waves is evident within each of the regions. Within the Eastern North Island, the attenuation rate is lowest in the direction of 30-60° from North, which is roughly along the strike of the subducting Pacific plate. A similar azimuthal dependence was also noted within the deep Central Volcanic Region, while the direction of lowest attenuation for waves originating in the shallow CVR is 5°.

Summary and Technical Abstract

Attenuation relations using weak ground motion recordings have been determined using data from the New Zealand National Seismograph Network and several temporary seismograph deployments. Models have been developed for earthquake sources in four regions: Eastern North Island Shallow; Eastern North Island Deep; Central Volcanic Region Shallow and the Central Volcanic Region Deep. Deep events were those with hypocenters below 33 km. Both volcanic and non-volcanic travel paths are considered. Regression coefficients have been determined for each of the regions using the attenuation models of Joyner and Boore (1981) and Molas and Yamazaki (1995). For example, for earthquakes in the Eastern North Island Shallow region, and excluding stations in the volcanic region, the resulting Joyner and Boore (1981) model equation is:

$$\log_{10} A = -5.56 + 0.983M - 0.0028r - \log_{10} r$$

where A is the peak ground acceleration in g, M is the local magnitude, M_L, and r is the hypocentral distance.

The attenuation is highest in the Central Volcanic Region. Anelastic attenuation rates (the coefficient of r above) for the shallow Central Volcanic Region are of the order of twenty times that observed for the Eastern North Island. Eastern North Island Deep attenuation rates are similar to Eastern North Island Shallow rates. The lowest attenuation rate was found for events within the Central Volcanic Deep Region, whose ray paths did not cross the Shallow Central Volcanic Region. This is consistent with a low rate of attenuation in the subducting Pacific plate.

Although the attenuation rate in the above Eastern North Island expression is comparable to that of Joyner and Boore (1981), the absolute level of the strong-motion attenuation curves greatly differs from those of the weak-motion, particularly at low magnitudes. This may be due to a number of factors. Unlike models within the literature, weak-motion far-field data have been used for this study, rather than strong-motion, near-field data. A second possible explanation for the difference in absolute level is the difference in frequency characteristics of large and small earthquakes. The corner frequency, f_c, and $f_{\max}$ describe the lower and upper frequencies respectively between which the acceleration spectra is flat. Above $f_{\max}$, the high frequency content of the waveform rapidly decays. With increasing magnitude, the corner frequency increases, while $f_{\max}$ remains constant. Thus it is possible that f_c might exceed $f_{\max}$ for low magnitude events. In this case the observed peak ground motion would be less than that expected for the magnitude of the event. Most importantly, differences may result from the use of M_L rather than the surface-wave magnitude, M_S, or moment magnitude, M_W, as are used in the strong motion models. The magnitude scale difference appears to be the primary reason for the difference in absolute level between the weak-motion and strong-motion relations. This means that while the constant and magnitude term in the above expression are different from strong motion models, the anelastic attenuation term should be directly comparable.

Azimuthal dependence of PGA is evident within each of the regions. Within the

Eastern North Island, the attenuation rate is lowest in the direction of 30-60° from North, which is roughly along the strike of the subducting Pacific plate. A similar azimuthal dependence was also noted within the deep Central Volcanic Region, while a slightly different minimum direction (5°) was determined for the shallow CVR.

Introduction

An accurate attenuation model is a crucial element of any seismic hazard study, as both design parameters and damage estimates are heavily influenced by the choice of attenuation model. In the past in New Zealand, models from either Japan or the US have been used because of insufficient local strong motion data. A best-average New Zealand peak ground acceleration attenuation model has recently been developed by Zhao et al. (1997) based on the available strong-motion data, but while regional variations were noted, they had insufficient data to define regional attenuation relations.

This report describes the use of the digital weak-motion database of the New Zealand National Seismic Network (NZNSN) to determine the attenuation of peak ground acceleration (PGA) on a finer scale than is possible with the strong motion data. While the motions considered are far below damaging levels, the variations in attenuation may have a bearing on strong-motion models. Most NZNSN stations are sited on bedrock, so the attenuation should be less contaminated by geological site effects. This is in contrast to the strong motion network which tends to be concentrated in population centres and therefore samples a wide range of site conditions.

Most PGA studies in New Zealand have made comparisons to overseas attenuation curves, particularly the western US (Joyner and Boore, 1981) or Japan (Fukushima and Tanaka, 1990), because of the limited strong motion data in New Zealand. Dowrick and Sritharan (1993a,b) looked at nine large New Zealand earthquakes and concluded that for events in all areas but Fiordland, there is a reasonable fit to the Japanese model, but the PGAs are much higher than in the western US model.

Most recently Zhao et al. (1997) developed attenuation relations for PGA for New Zealand earthquakes of M_w = 5.1 - 7.4. They considered the effects of depth, focal mechanism, ground class and tectonic type (crustal, interface or dipping slab). 51 New Zealand earthquakes were used for that modelling, supplemented by 17 overseas events in the near field. Overall, events which occur along the plate interface give rise to smaller PGA's than crustal or slab events. Regional differences of PGA attenuation rates for Fiordland and the CVR compared to the rest of New Zealand were also investigated. Data from Fiordland events suggest that PGA's in this region are higher for a given set of parameter values that elsewhere in the country. Travel paths within the CVR were found to experience a higher rate of attenuation that other areas of New Zealand but there were insufficient data to determine regression parameters.

Spectral attenuation studies in New Zealand are limited due to a lack of strong motion data, but seem to agree with Japanese data (McVerry, 1986). Matuschka and Davis (1991) made a first attempt at a spectral attenuation relationship using New Zealand data but caution that their model still needs to be considered in relation to overseas models.

Many studies of attenuation in New Zealand have used intensity data because it was available for the largest events. Smith (1978), using isoseismal maps of 68 earthquakes, separated New Zealand into 3 separate regions, each with its own set of attenuation curves. He also defined the ellipticity of the isoseismals for each region. Dowrick (1991b) revised the attenuation relationships using new magnitudes and including a depth factor. He used circular isoseismals and did not find a regional variation in attenuation except for the Central Volcanic Region (CVR) and perhaps Fiordland. Satake and Hashida (1989) inverted for the 3D attenuation structure of the North Island using the intensities of 26 earthquakes. They found a low Q in the CVR and a high Q in the subducting slab. The differences in the Smith and Dowrick models have important implications for seismic hazard assessment, particularly whether there are azimuthal and regional variations in intensity.

New Zealand was also divided into a small number of regions based on the amplitude attenuation studies of Haines (1981) that were part of his updating of the New Zealand local magnitude scale. Ray paths for crustal earthquakes were assigned the same attenuation unless they traversed the Central Volcanic Region. Subcrustal earthquakes were divided into 2 groups: the main seismic zone and the region to the south of the main seismic zone.

This report, which is based on Aasha Pancha's MSc thesis research, addresses the variability of attenuation relations primarily within the eastern North Island and the Central Volcanic Region of New Zealand. The data selection and processing will be described followed by an explanation of the form of the attenuation relations used in the study. Then the results of the regression analyses and their implications will be discussed, including the consideration of azimuthal effects.

Data Selection

The New Zealand National Seismograph Network (Figure 1) was upgraded to digitally recording stations in the late 1980's and early 90's. As seen in the figure, the station distribution is rather sparse with an average spacing of about 100 km. To increase the density of attenuation data, recordings from temporary deployments operated by the Institute of Geological and Nuclear Sciences (IGNS) near East Cape and Marlborough in 1993-1994, and the Taupo Volcanic zone in 1995 (TVZ-95) were included in the data set. Station spacing within the temporary deployments was about 10-50 km. Figure 2 shows the location and distribution of stations of these three temporary deployments. In addition, a few station recordings from other temporary deployments were also included (Figure 1).

Earthquakes from the IGNS National Catalogue were considered if their magnitude was > 3.0 and their location was within the Eastern North Island (ENI) or Central Volcanic Region (CVR) (based on the regions defined by Smith and Berryman, 1983)(Figure 1). Within each region, data were classified as either shallow ($\leq$ 33 km) or deep. Thus the data have been separated into four different regions for analysis: the Eastern North Island shallow (ENIS); Eastern North Island Deep (ENID); CVR shallow (CVRS); and CVR deep (CVRD).

Events were selected if they were recorded on a large number of three component

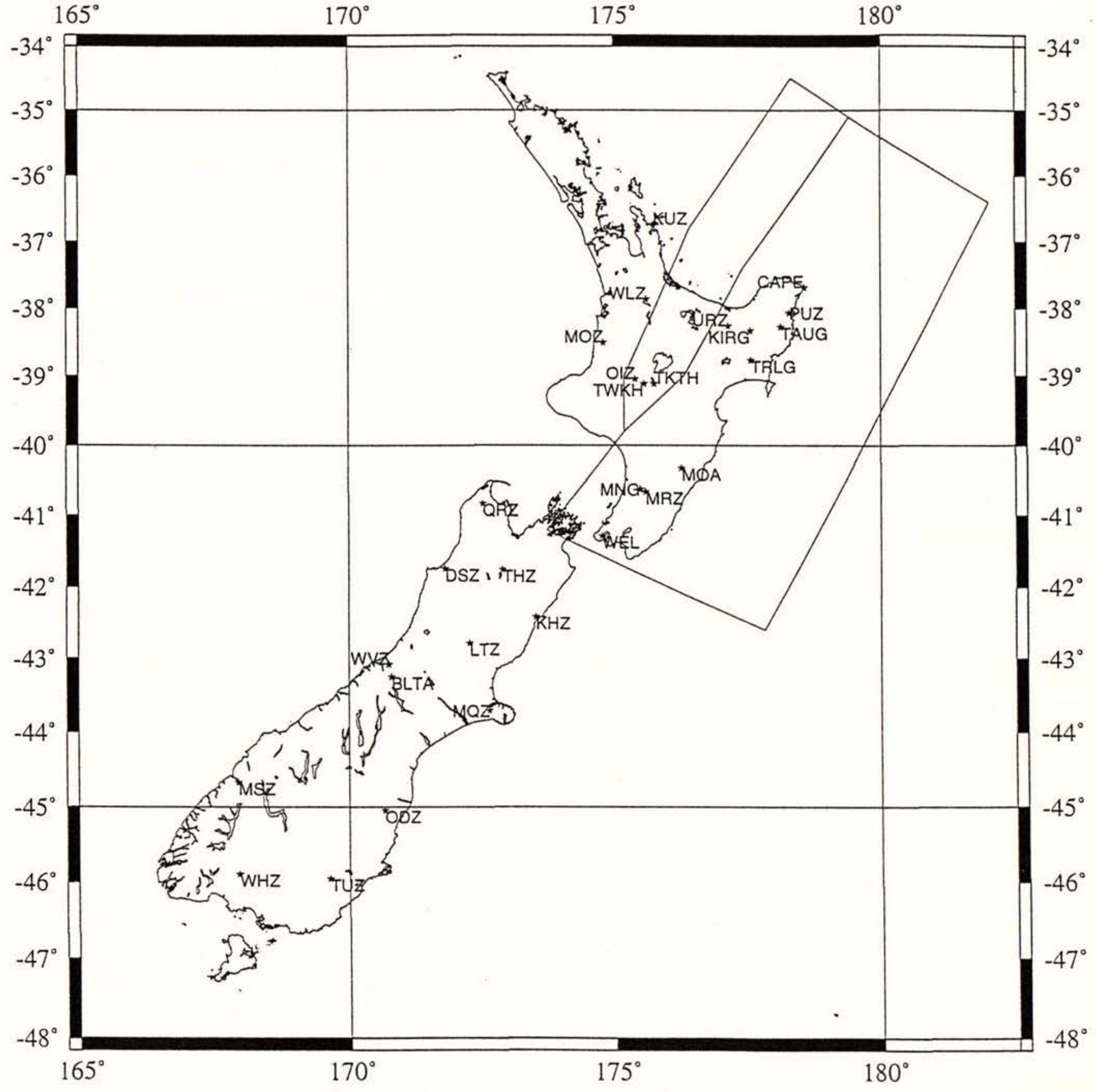

Figure 1. New Zealand National Seismograph Network. Map showing locations of the three component EARSS digital stations installed during the time interval of this study. The location of the Eastern North Island and Central Volcanic Regions are superimposed. The regions are based on those of Smith and Berryman (1983). Location of temporary EARSS stations included in this study are also shown. These stations are the following: the East Cape EARSS: CAPE; the Alpine experiment: BLTA; Tony Hurst's temporary stations: TWKH, TKTH; and the Ormondville temporary stations: KIRG, TAUG, TRLG.

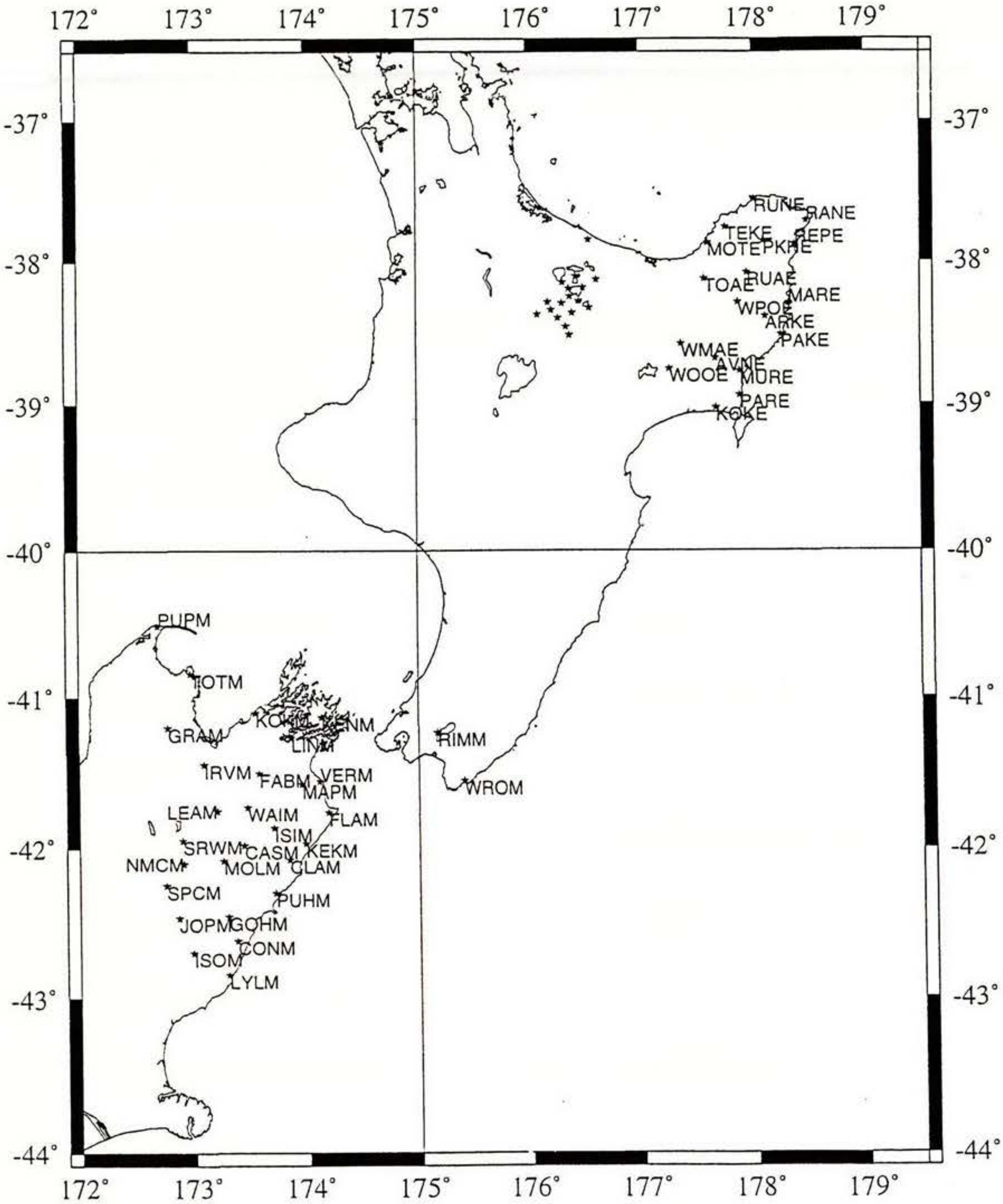

Figure 2. Map showing station locations of the PANDA deployments in East Cape and Marlborough, and the TVZ95 Taupo Volcanic Zone deployment.

stations, either because of their large magnitude or because of their proximity to a dense portable deployment. Locality of events was a secondary criterion for data selection to ensure data were well distributed spatially within each region.

In total, 110 events were analysed: 32, 25, 24 and 29 events respectively for the CVR deep, CVR shallow, Eastern North Island deep and Eastern North Island shallow regions. Figures 3 and 4 show the event distribution for each of these regions, while Appendix 1 lists the location, depth and magnitude of each event. Events have not been classified on the basis of source mechanism because the mechanisms for most of the events used in this project have not been determined. This lack of classification will add a little to the scatter of the data since source mechanisms have been shown to be a factor in PGA (Dowrick and Sritharan, 1993a,b; Zhao et al., 1997).

Data Processing

Waveforms from the selected events were first extracted from the IGNS earthquake catalogue. The processing steps included converting between data formats (CUSP at IGNS to AH at VUW), removing the instrument response of the the velocity sensor, and then converting from velocity to acceleration. Only sites with EARSS recording systems (Gledhill et al, 1991) were considered so that the system response was the same for all sites.

Only horizontal components were considered because of the greater engineering significance of horizontal motions. Although the traces for each earthquake event were processed in bulk, traces for each individual station were visually checked before any processing was done. This was in order to check firstly that the traces contained an S phase. Also if the background noise was too high, the trace was not processed. As discussed later, once the processing had been completed, the signal to noise ratio of each trace was checked. Once the traces had been manually checked and trimmed, the waveforms were processed in bulk.

We developed a processing technique for converting the waveform data to accelerations. At the first stage of the conversion, the traces were de-meaned and tapered using a 10% parzen taper. The instrument response was then removed from each of the waveforms. The deconvolution included a third order high pass filter at 0.5 Hz. The waveforms were then once again tapered. Following the removal of the instrument response the waveforms represented the true velocity function with time. The derivative of the velocity function was then computed by the spectral method, to obtain acceleration traces in m/sec^2. A low-pass 25 Hz butterworth filter was then applied.

Once this processing had been completed, each individual trace was once again viewed. This was to ensure that the maximum value was indeed the true maximum acceleration and that the traces were not dominated by noise. Some traces included constant background noise or noise spikes which could overshadow the true maximum value. If they did overshadow the true value, the trace was eliminated. If not, the segment containing the true peak value was extracted. Individual components

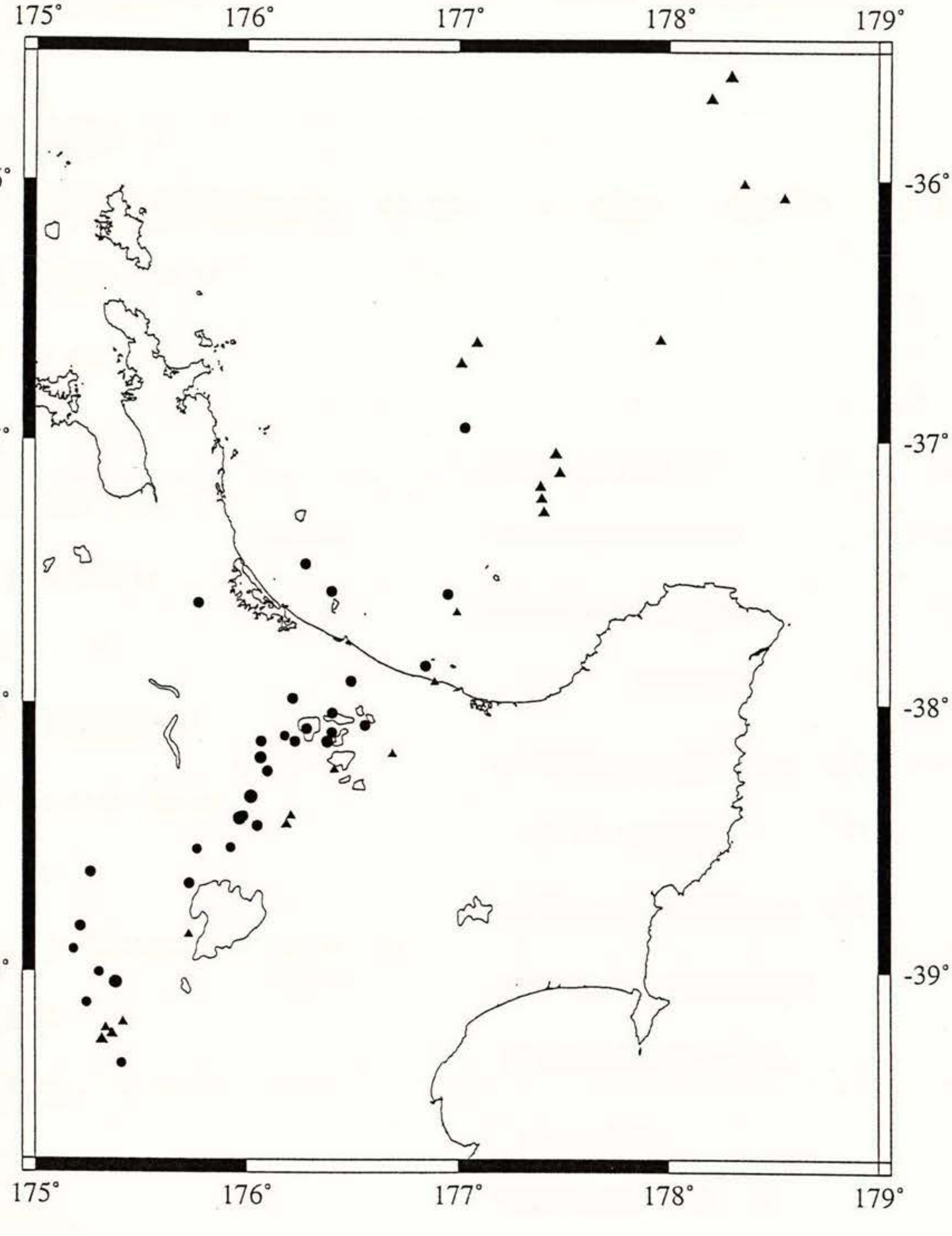

Figure 3. Earthquake locations within the Central Volcanic Region. The CVRD events are represented by a square, while those of the CVRS are represented by a triangle. Magnitudes range from 3.8 to 5.4 for the CVRD and from 3.3 to 5.4 for the CVRS. These events are listed in Appendix 1.

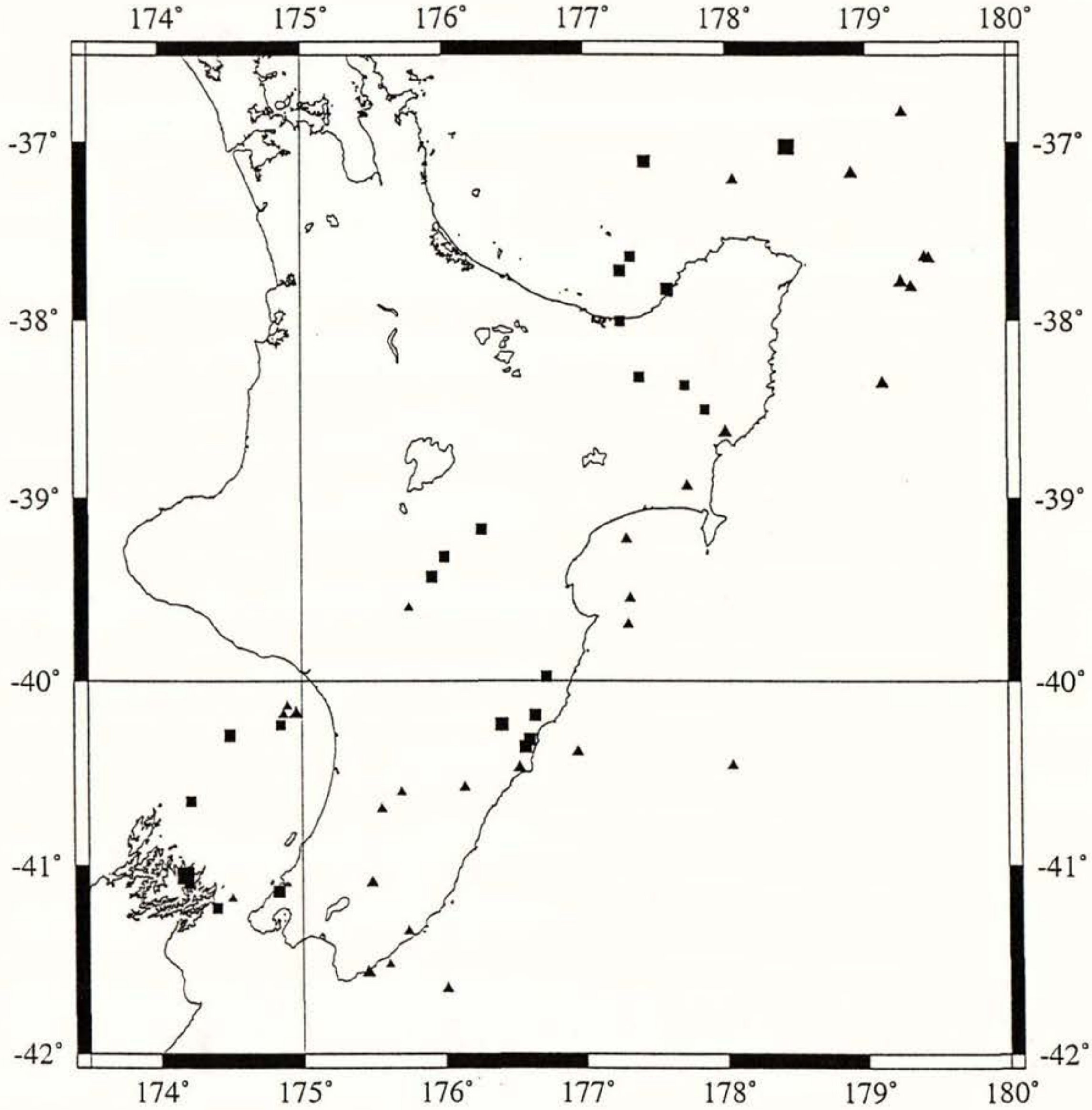

Figure 4. Earthquake locations within the Eastern North Island Region. The ENID events are represented by a square, while those of the ENIS are represented by a triangle. Magnitudes range from 3.3 to 6.5 for the ENID and from 3.2 to 5.1 for the ENIS. These events are listed in Appendix 1.

of each station were then written to individual files so that the peak ground acceleration and signal to noise ratio could be automatically read. The signal to noise ratio was calculated for each of the horizontal components. Stations with a signal to noise ratio of less than four were eliminated. Some traces with signal to noise ratios of 4.0 - 4.5 were also eliminated if the background noise looked to be masking the seismic signal. Traces with a sampling rate of 25 Hz were also eliminated, as much of the peak energy would be absent. In general, the NZNSN stations have a sampling rate of 50 Hz. The PANDA deployment stations however had a sampling rate of 100 Hz.

The peak value of each horizontal component was picked and both the maximum of the two components and root mean squared values of the two components for each station were tabulated. In total there were 2212 traces; 745, 240, 605 and 598 records respectively for the CVR deep, CVR shallow, Eastern North Island deep and Eastern North Island shallow regions. Figure 5 shows plots of the distance distribution of the four regions of this study. At large distances the data become sparse. For this reason, and to minimise bias due to untriggered (null observations) and non-operational stations, data for each of the four regions have been truncated at a distance of 500 km. This reduced the total number of traces to 1908, corresponding to an average of about 17 traces per event. The acceleration distribution for each region for the truncated data set is shown in Table 1.

Table 1. Distribution of data used for the regression analyses

Acceleration (g)			Hypocentral Dist. (km)			Mag. (Ml)		
Central Volcanic Deep								
1.19e-06	to	0.00235	108	to	499	3.7	to	5.5
Central Volcanic Shallow								
1.33e-06	to	0.00196	20	to	449	3.3	to	5.4
Eastern North Island Deep								
1.32e-06	to	0.0254	34	to	495	3.3	to	6.5
Eastern North Island Shallow								
1.23e-06	to	0.00760	28	to	493	3.1	to	5.1

Acceleration Comparisons

It was necessary to ensure that the conversion of the CUSP velocity data to acceleration was in agreement with the acceleration measured on strong motion instruments. In order to do this, comparisons between earthquake data recorded simultaneously on an EARSS seismograph and an adjacent strong-motion accelerograph were made independently by IGNS and in the current study. The instruments were operated by IGNS at the Seismological Observatory, Kelburn for a five month period. Six events of sufficient size (Table 2) were used in the comparison.

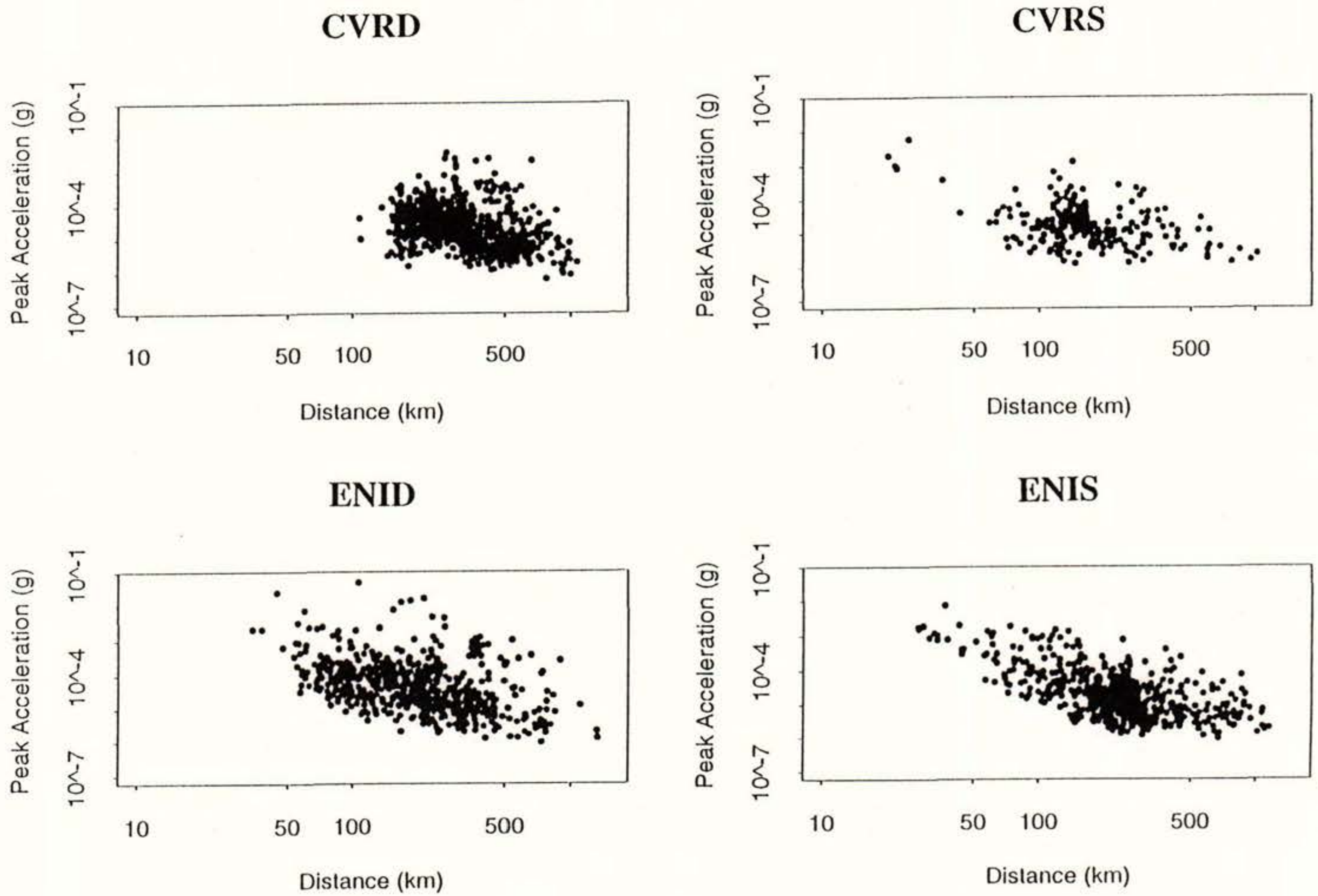

Figure 5. Distribution of acceleration data with distance within each of the four regions. CVRD = Central Volcanic Region (Deep); CVRS = Central Volcanic Region (Shallow); ENID = Eastern North Island (Deep); ENIS = Eastern North Island (Shallow). Data beyond 500 km were not used in the regressions.

Table 2. Earthquake data used to compare PGA obtained from seismographs with those of accelerographs. Data from the last three events are later used to compare regressions using M_L and M_S.

Date	Lat	Long	Ml	Ms	Depth (km)	Hypo. Dist. (km)
Dec 15 1994	-40.8280	175.1245	5.27		28.4	65.5
Dec 20 1994	-40.5074	174.9876	4.64		54.9	104.2
Jan 06 1995	-41.3016	174.2950	5.18		69.3	79.8
Feb 05 1995	-37.6496	179.4886	6.98	7.50	12.0	572.4
Feb 10 1995	-37.9157	179.5141	6.52	6.50	12.0	552.9
Mar 22 1995	-41.0523	174.1805	6.47	5.80	90.3	106.1

In the current study, the seismograph data were processed in the same manner as that of the main data set. The resultant PGA values were compared with those of the accelerograph which were supplied by IGNS. At most, discrepancies between the two values of PGA were within 12% of each other with five of the six measurements having less than 5% difference. A similar comparison was made of data from weight drops at the new Museum of New Zealand (MONZ) site, Wellington, where a difference of at most 10% was observed.

The comparison of the two instrument types conducted by IGNS was carried out in order to investigate the possibility of supplementing their strong-motion database of rock site recordings with velocity data from the NZNSN. The EARSS data were processed in a slightly different manner to that of the current study. Processing consisted of conversion from velocity to acceleration in the frequency domain, correction for the response of the L4C transducer, and high-pass filtering at 0.5 Hz. The processing methods used by IGNS and this study gave very similar values of acceleration with at most a 5% difference. In addition to this, a data set of 295 rock-site PGA's from seismograms recorded between 1990 and 1995 were compared with strong-motion rock-site data. Statistical analyses of these two data sets showed that the variance of the seismograph rock-site data was greater than that of the strong-motion data from all sites (Jim Cousins, personal communication, 1996).

Accelerograph data are not used within this study. However, the above analysis demonstrates that PGA derived from the conversion of velocity data from the NZNSN are comparable to the PGA determined from strong ground motion instrumentation.

Regression Analysis

For this study of far-field, weak motion attenuation, the models and methods of Joyner and Boore (1981) and Molas and Yamazaki (1995) have been adopted. The Joyner and Boore (1981) model was selected because it is based on the attenuation of body waves in an elastic medium from a point source. The Molas and Yamazaki (1995) model was chosen for the same reason, and because it includes both a depth term and a constant term for each recording station. Moreover, Molas and Yamazaki

(1995) used data from Japan, which has a similar tectonic environment to New Zealand. The use of the Molas and Yamazaki (1995) model allows a direct comparison of the Japanese data and the current data set.

Parameters

Two definitions of the independent variable, the horizontal acceleration, have been regressed for. Traditionally peak ground acceleration is usually preferred (Molas and Yamazaki, 1995; Joyner and Boore, 1981; Bolt and Abrahamson, 1982; Ambraseys and Bommer, 1991). However, peak values often vary greatly between the orthogonally orientated horizontal components. For this reason the regressions were also determined using the root-mean-squared of the peak values of the two horizontal components. No significant difference between the two measures of acceleration were noted.

The distance between the recording sites and the energy source of the weak motion is generally of the order of 100 km or more. Unlike strong motion studies, this removes the problem of stations being closer to some part of the fault rupture than the initiation of energy release. As a result, the hypocentral distance, as calculated from the IGNS catalogue location, has been used in this study.

Since 1977, New Zealand earthquakes have been classified using a local magnitude scale. The scale is a revised definition of Richter's original scale based on the characteristics of seismic attenuation beneath New Zealand (Haines, 1981). Hence, M_L has been adopted as a measure of earthquake size throughout this study as values were available for all weak motion events, whereas M_W and M_S values are only available for selected strong motion events. As discussed later, the choice of magnitude scale may have an effect on the resulting regression constants.

The Joyner and Boore Two Stage Regression

The two stage regression of Joyner and Boore (1981) is the primary technique used for deriving attenuation models in this study. The technique was favoured because of its simple model and because the method decouples the distance dependence from the magnitude dependence.

The Joyner and Boore model is as follows:

$$\log_{10} y = c + aM + br - \log_{10} r + dS.$$

For this study y is either the maximum or root mean squared horizontal acceleration in g, r is the hypocentral distance in kilometres and the station term, $S = 0$ as all stations are located on hard rock. The $\log_{10} r$ term accounts for geometric spreading while br is the anelastic attenuation term.

The Molas and Yamazaki Regression Model and Method

In addition to the Joyner and Boore (1981) attenuation model, the regression model and method of Molas and Yamazaki (1995) was applied. The form of their model is as follows:

$$\log_{10} y = b_0 + b_1 M + b_2 r + b_3 \log_{10} r + b_4 h + c_i,$$

where

y	=	acceleration in cm/s^2
M	=	is the magnitude
r	=	is the distance in km
h	=	is the depth in km
c_i	=	is the station coefficient of the ith recording station.

In addition to the terms adopted by Joyner and Boore (1981), Molas and Yamazaki (1995) include a depth term and station terms which are calculated through the use of dummy variables (Draper and Smith, 1981). From preliminary analyses, Molas and Yamazaki (1995) showed that both the depth term and the station term significantly improved the fit of the regression model. A positive correlation between the residuals and depth were noted when the depth term was omitted. When the depth term was incorporated, the R^2 statistic significantly improved and the standard error reduced.

Although the recording stations of this study are located on hard rock, local geological and topographic variations result in differences in site amplification. Thus to gain a better fit to the attenuation data and a better understanding of recording site influences, the inclusion of a station term for this study is desirable.

The statistical computer package **S-PLUS** was used to derive the regression equations. **S-PLUS** is a language and an interactive programming environment for data analysis and graphics (see Chambers and Hastie, 1992; Venables and Ripley, 1994). The simple linear regression was achieved using the **lm** function for fitting linear models. The function uses the principle of least squares to minimise the sum of squared residuals.

Regression Results and Discussion

Complete Data Set

The derived attenuation models for the complete data set for each of the four regions are listed in Table 3, while Table 4 summarises some of the attenuation relations from the literature to which comparisons are made. The effectiveness of fitting a regression model is often discussed in terms of the R^2 statistic. However this statistic has a number of poor properties and can at best be taken as a general indication of the nature of the fit. For example, augmenting the set of predictor variables by

Table 3. Derived attenuation coefficients for the ENID, ENIS, CVRD and CVRS regions.

Data Set †	constant	M	log_{10} r	r	depth
	Eastern North Island Deep				
JB_{max}	-4.7777	0.7725	-1	-0.00248	—
MY_{max}	-2.2474	0.8744	-1	-0.0027	0.00112
	Eastern North Island Shallow				
JB_{max}	-4.3111	0.6304	-1	-0.00281	—
MY_{max}	-2.3216	0.8231	-1	-0.0026	0.0030
	Central Volcanic Region Deep				
JB_{max}	-4.4624	0.5109	-1	-0.00013	—
MY_{max}	-2.8272	0.9353	-1	-0.0014	-0.0011
	Central Volcanic Region Shallow				
JB_{max}	-5.0075	0.6830	-1	-0.00205	—
MY_{max}	-2.1831	0.7798	-1	-0.0044	-0.0142

† Note that coefficient of the $\log_{10}$ term has been constrained to -1 in each case. The coefficient of the distance term of the Joyner and Boore (1981) type regressions are rounded to 5 decimal places while all other coefficients are rounded to four decimal places. (max = maximum accelerations, JB = Joyner and Boore (1981) model and method (in g), MY = Molas and Yamazaki (1995) model and method (in cm/s^2))

Table 4. Attenuation relations from the literature.

Joyner and Boore (1981)§	$\log_{10} A = -1.02 + 0.249M - \log_{10} R - 0.00255R$
Ambraseys and Bommer (1991)§	$\log_{10} A = -1.09 + 0.238M - \log_{10} R - 0.0005R$
Molas and Yamazaki (1995)¶	$\log_{10} A = 0.206 + 0.477M - \log_{10} R - 0.00144R - 0.00311H$
Fukushima and Tanaka (1990)¶	$\log_{10} A = 1.30 + 0.41M - \log_{10}(R + 0.032 \cdot 10^{0.41M}) - 0.0034R$
Zhao *et al.* (1997)§ Model 5	$\log_{10} = -0.490 + 0.331M - 1.59 \log_{10}(R^2 + 20^2)^{1/2} + 0.00566H$

§ Accelerations are in g.
¶ Accelerations are in cm/s^2.

any new variable whatsoever will cause the R^2 value to increase, apparently giving a better model. This, and other properties (Brook and Arnold, 1985; Weisberg, 1985), imply that statistical comparisons between the Joyner and Boore (1981) and Molas and Yamazaki (1995) models are not particularly feasible. Using the standard error is prone to similar problems.

More importantly, the residuals of a model obtained through an ordinary one-stage least squares procedure may differ greatly from those obtained via the two and three stage procedures used here. In addition, the fit of the model at each stage of the regression processes has no bearing on the overall fit of the resultant relation (Brian Dawkins, personal communication). However, since the statistics are commonly used in the seismological literature (eg. Fukushima and Tanaka, 1990; Matuschka and Davis, 1991; Molas and Yamazaki, 1995; Zhao et al., 1997) they are included here (Table 5).

One expects that the anelastic attenuation term (the distance term) will increase with increasing attenuation along the ray path. Anelastic losses are greatest in the shallow section of the crust (Atkinson, 1995). We therefore expect that the relations obtained for the shallow data subsets will yield anelastic attenuation coefficients (coefficient of r in Table 3) that are larger (more negative) than those of the deep data subsets. From Table 3 we see that the anelastic coefficient of the CVRS data is significantly larger than that for the CVRD, as expected. However, the anelastic coefficient of the CVRD data is almost zero when the Joyner and Boore (1981) model is applied. Moreover, those of the Eastern North Island are larger than those obtained for the CVRS. This is contrary to the expected results.

Analysis of the data showed that data pertaining to the Eastern North Island and TVZ-95 deployments were associated with a large degree of scatter. Over short distance ranges, data from these deployment stations had a large variation in PGA (Figures 6 and 7). This was not totally unexpected. While stations of the NZNSN are located on the hardest rock type within the region, those of the short term deployments are less likely to be. As a result, site conditions vary greatly from station to station. This gives rise to the scatter observed. The same effect is not noted within the Marlborough deployment, probably because these stations are situated on older, higher grade metamorphic rocks. These rocks are more consolidated than the sedimentary and volcanic deposits within the Eastern North Island and Taupo regions.

These scattered data values greatly influence the regressions. To allow for these data points, the regression curves are forced to pass through the center or the most concentrated portion of these clusters (Figures 6 and 7). In order to correct for this effect it was decided to further segregate the data to eliminated this effect and to further quantify the effects of the Central Volcanic Region.

Preferred Models

Data from the East Cape deployment were completely removed from each of the data sets. The data sets for each of the four regions were then further divided, each data

Table 5. R^2 statistics and standard error of each stage of the regressions. The non-volcanic dataset will be discussed in a later section.

Model	Stage 1		Stage 2		Stage 3	
	R^2	S.E.	R^2	S.E	R^2	S.E
			Eastern North Island Deep			
JB_{max}	0.9689	0.3910	0.9105	0.1820	—	—
MY_{max}	0.7895	0.2464	0.9613	0.2659	0.9708	0.1153
$JB_{non-volcanic}$	0.9726	0.3707	0.9483	0.1671	—	—
$MY_{non-volcanic}$	0.7553	0.2546	0.9676	0.2146	0.9550	0.1548
			Eastern North Island Shallow			
JB_{max}	0.9733	0.4073	0.8358	0.1699	—	—
MY_{max}	0.7011	0.3097	0.8865	0.2495	0.9112	0.1563
$JB_{non-volcanic}$	0.9784	0.3831	0.8363	0.2685	—	—
$MY_{non-volcanic}$	0.6076	0.3467	0.8457	0.2589	0.8433	0.2554
			Central Volcanic Region Deep			
JB_{max}	0.9651	0.4341	0.4884	0.2192	—	—
MY_{max}	0.8604	0.2032	0.9706	0.1677	0.9386	0.1003
$JB_{non-volcanic}$	0.9791	0.3526	0.7646	0.2361	—	—
$MY_{non-volcanic}$	0.3149	0.3708	0.882	0.3237	0.7865	0.2255
			Central Volcanic Region Shallow			
JB_{max}	0.9746	0.4397	0.6765	0.2632	—	—
MY_{max}	0.6935	0.3166	0.8557	0.2286	0.8134	0.2082
$JB_{non-volcanic}$	0.9814	0.3931	0.6956	0.3044	—	—
$MY_{non-volcanic}$	0.7769	0.3169	0.9674	0.2297	0.9247	0.1800

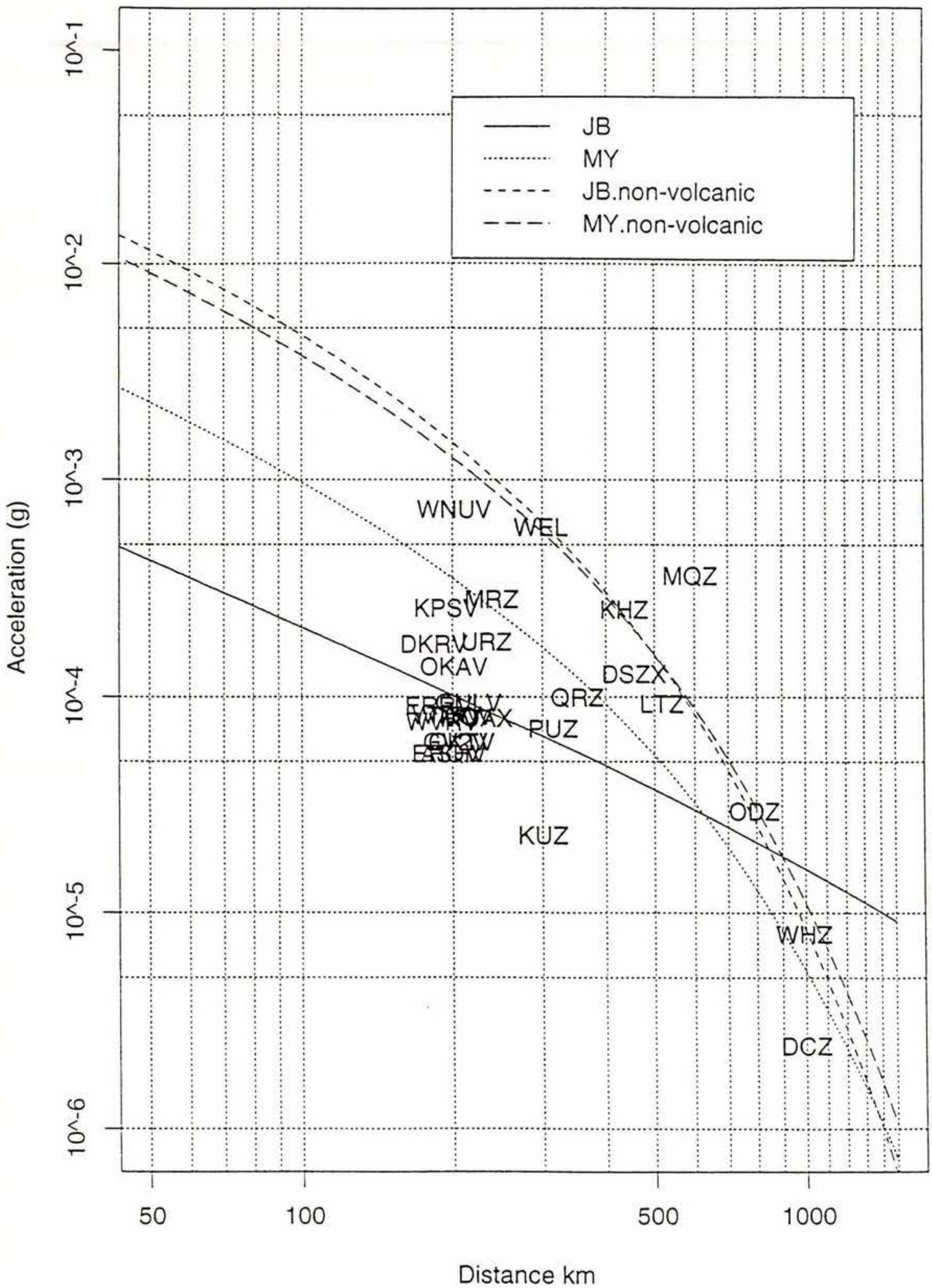

Figure 6. Comparison of derived CVRD attenuation relations with a CVRD event of M_L = 5.5 and depth = 156 km. Note the scatter of data from the Volcanic Deployment stations. The non-volcanic attenuation curves were derived by excluding stations within the CVR and the East Cape Deployment. Stations beyond 500 km were not used in the regressions.

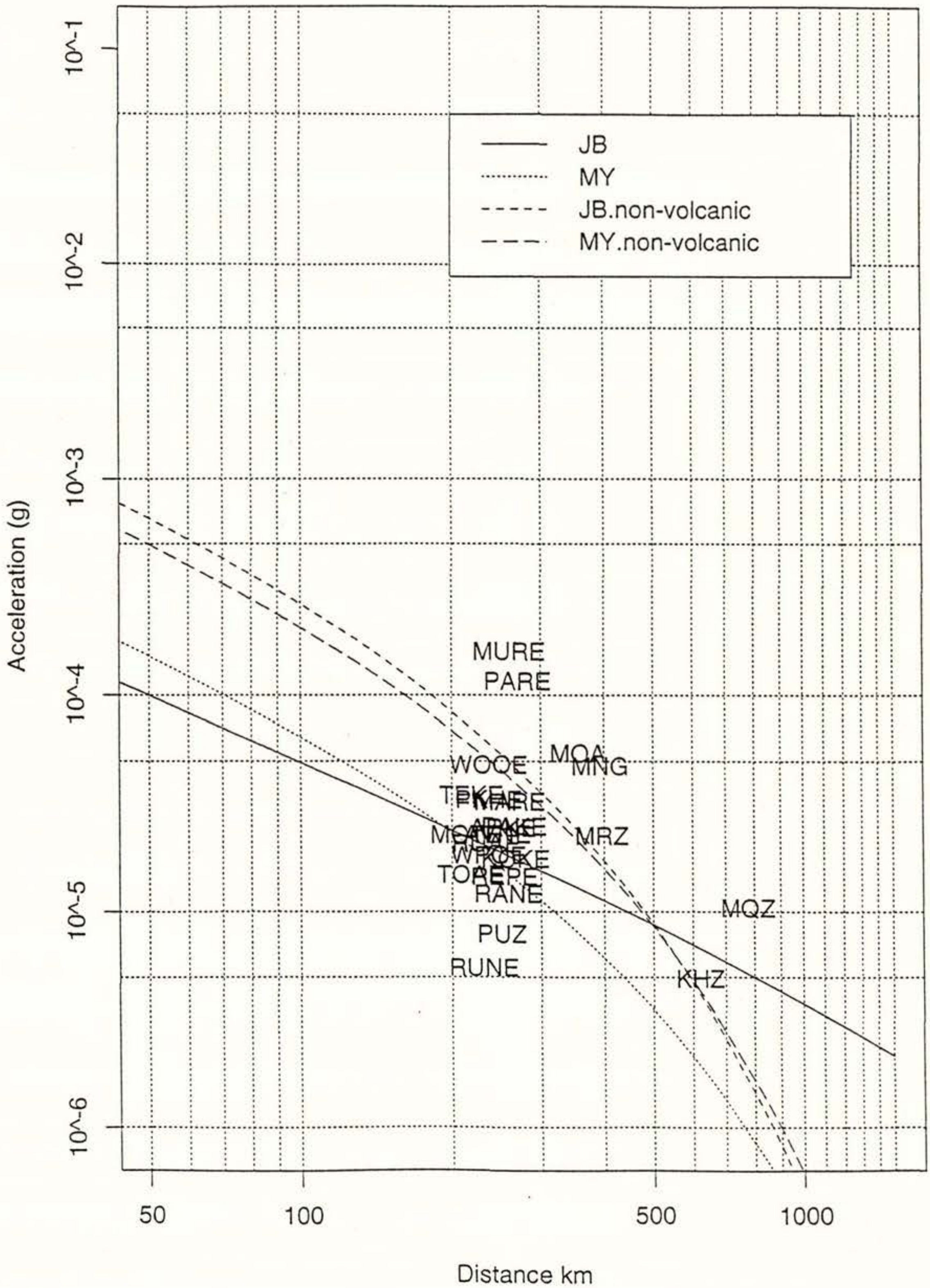

Figure 7. Comparison of derived CVRD attenuation relations with a CVRD event of $M_L = 4.2$ and depth = 182 km. Note the scatter of data from the East Cape Deployment stations. The non-volcanic attenuation curves were derived by excluding stations within the CVR and the East Cape Deployment.

set being separated into two classes. The first class comprised data which had not experienced attenuation effects of the shallow Central Volcanic Region. It included stations from the Marlborough deployment as well as most the NZNSN stations. The stations KUZ, MOZ, OIZ and WLZ were eliminated as any waves travelling to these stations must pass through the Volcanic Region. This dataset is hereafter referred to as the "non-volcanic" dataset. Note that there is no CVRS region in this dataset.

The second class comprised earthquake recordings for which ray paths pass through the Central Volcanic Region. Thus the data is referred to as the "volcanic" dataset. Recording stations of this class included the four NZNSN stations, KUZ, MOZ, OIZ and WLZ, as well as three of the TVZ-95 deployment stations (DKRV, GV2V and OKAV). Only three stations from the deployment were selected because of the problem of scatter. The three stations were chosen because they seem to be more consistent, and because they recorded a larger number of the events than other stations within the deployment.

Regressions using both the Joyner and Boore (1981) method as well as the Molas and Yamazaki (1995) method were performed on the non-volcanic dataset. As some events only contained one data record, these were removed from the magnitude dependent regressions following Joyner and Boore (1981) The resultant attenuation models are shown in Table 6. The effect of removing the East Cape deployment stations and the volcanic ray paths is significant. The fit of the main trend of the data is improved, especially so for the CVRD Joyner and Boore (1981) type regression (Figures 6 and 7). The rates of anelastic attenuation in the ENIS and ENID regions are every similar to each other. Thus for the distances considered in this study, the rate of attenuation from earthquakes occurring in the upper 33 km of the crust is comparable to that of earthquakes occurring below 33 km within the Eastern North Island region. Attenuation rates of the CVRD, where earthquakes originated within the subducting slab, are much less. This confirms the hypothesis that seismic waves travelling through the subducting Pacific Plate experience much less attenuation than those travelling through the overlying crust.

It has been known that attenuation rates within the Central Volcanic Region are high (eg. Zhao et al., 1997; Mooney, 1970). Analysis of the volcanic dataset, for which events have been recorded within the Central Volcanic Region, allowed the influence of the Central Volcanic Region to be quantified. Because the volcanic dataset was so sparse, only the first stage of the traditional Joyner and Boore (1981) method was applied to gain the anelastic attenuation rate (the coefficient of r in Table 7). As is seen in Table 7, the computed attenuation rate for the CVRS (-0.067), is significantly higher than those of the other three regions. Thus the anelastic attenuation is greatest for ray paths that pass solely through the shallow Central Volcanic Region. Waves travelling from the Eastern North Island regions into the shallow CVR have similar but slightly higher rates of anelastic attenuation than waves travelling from the CVRD up to the shallow CVR (Table 7). In the case of the ENIS events, this reflects the fact that these ray paths pass through the shallow crust of the Eastern North Island in addition to the shallow crust in the CVR. The

Table 6. Attenuation coefficients for the non-volcanic dataset. JB models are for accelerations in g, MY models are in cm/s^2.

Data Set	constant	M	log_{10} r	r	depth
Eastern North Island Deep					
JB_{max}	-5.271	0.9444	-1	-0.00272	—
MY_{max}	-2.2497	0.9408	-1	-0.0027	0.0001
Eastern North Island Shallow					
JB_{max}	-5.5615	0.9826	-1	-0.00280	—
MY_{max}	-2.7833	0.9594	-1	-0.0026	0.0050
Central Volcanic Region Deep					
JB_{max}	-5.6905	1.0149	-1	-0.00194	—
MY_{max}	-2.9414	1.032	-1	-0.0017	0.0002

Table 7. Calculated anelastic attenuation rates (the coefficient of the r term) to stations in the CVR from each of the four regions (the "volcanic" dataset).

Region	Attenuation Rate
ENID	-0.00750
ENIS	-0.00813
CVRD	-0.00718
CVRS	-0.0673

slightly higher anelastic attenuation in the ENID region than the CVRD region shows that anelastic attenuation in the CVR must be primarily in the shallow crust. If high rates of attenuation extended deep beneath the CVR, the CVRD anelastic attenuation rate should be greater than the ENID rate.

The average rate of anelastic attenuation for non-volcanic ray paths in the Eastern North Island region (Table 6) is only about -0.003 g/km. Thus the anelastic attenuation rate for paths entirely within the CVRS (0.067) is over twenty times higher than the rate for non-volcanic paths.

Depth Term

One expects that the addition of the depth term, and in particular, the station constant terms in the Molas and Yamazaki regression, would significantly improve the residuals of the Joyner and Boore attenuation model. Table 6 shows that the addition of the terms alters significantly the values of the coefficients of the original terms. Nevertheless the predicted ground motions are very similar to the Joyner and Boore model (Figures 6 and 7). The effects of the station term are clear, but the physical significance of the depth term is not fully understood (Molas and Yamazaki, 1995).

From Table 6, we see that the value of the depth coefficient decreases with increasing depth of the seismic source. This was also noted by Molas and Yamazaki (1995). Deep events propagate through high-Q zones, hence the depth term may correct for the lower rate of attenuation (Molas and Yamazaki, 1995). The depth coefficient of the CVRD for the whole dataset is negative in value (Table 3). Molas and Yamazaki (1995) also obtained a negative depth coefficient for earthquakes 90-120 km in depth. They concluded that this may be due to insufficient data. For this study, the negative depth coefficient is more likely to be an artifact due to the large degree of scatter within the data.

Station Terms

The station terms account for the fact that some stations have consistently greater or smaller PGA than that of the main trend. These differences are mainly due to site conditions and path effects. Appendix 2 lists the station terms for each region for the Molas-Yamazaki regressions for the complete data set and the non-volcanic data set. For example, the station MQZ is consistently much higher than the trend than any other station, particularly for the ENID (Figure 8). It therefore has a much more positive station term than any other station, as expected. Stations which lie much lower than the trend likewise have negative station terms.

The values of the station coefficients are not consistent with those of the travel time corrections used by IGNS for earthquake location. Comparisons show that the attenuation station terms for individual stations vary depending on the source region. This means that the attenuation station terms include a partial path effect

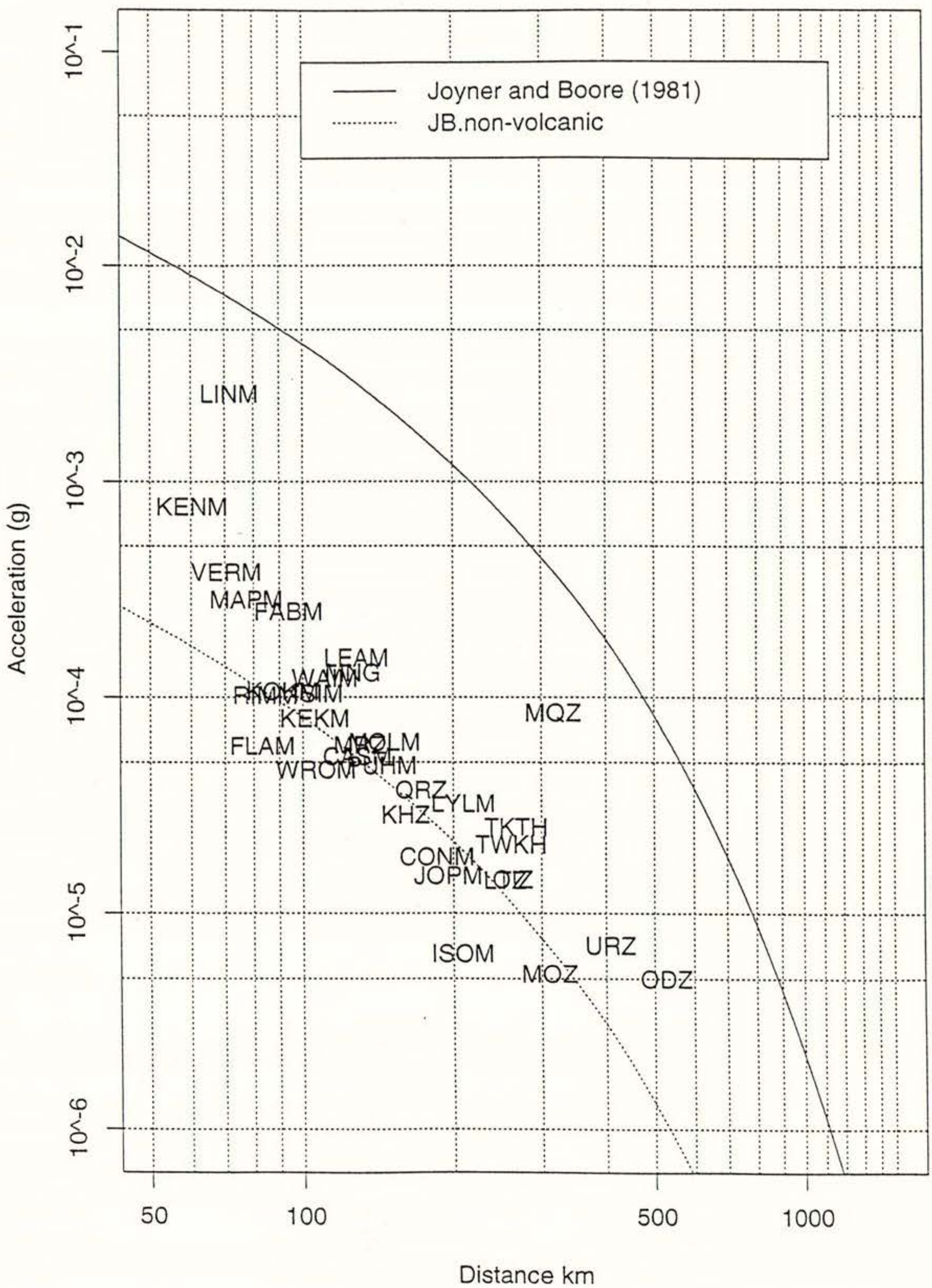

Figure 8. Comparison of the JB non-volcanic and the Joyner and Boore (1981) attenuation models with an ENID event of M_L = 3.65 and depth = 55.2 km. The difference in absolute level between these two models greatly increases at low magnitudes (compare with Figures 9 and 10), but the rate of anelastic attenuation is seen to be similar for the two models. The data also demonstrate the application of the Molas-Yamazaki station terms. Note that MQZ lies significantly above the main trend of the data. As seen in Appendix 2, MQZ has a highly positive station term to account for this, particularly for the ENID.

as well as a site effect, whereas the travel time corrections should include only the local site effect. This was evident for those stations within the CVR. The effect of the greater attenuation through the volcanic region was to a degree reflected in negative station terms. In particular, station terms derived for these stations for earthquakes within the CVRD are highly negative reflecting the difference between the low-attenuation slab paths and paths through the Central Volcanic Region.

The effect of the station terms were less evident for those stations of the Eastern North Island deployment. As discussed above, stations from the East Cape Deployments were associated with a large degree of scatter. If the scatter of station amplitudes were consistent from event to event, it would be expected that the station terms would be of the same order as the scatter. However the Eastern North Island station terms exhibit much less variation than seen in an individual event (Figure 7). This implies that the scatter must be at least partially a path effect and not only a site effect.

Comparison to overseas and New Zealand strong-motion relations

The strong motion relations were developed from data recorded in the near-field from large magnitude events (Table 8). This is in contrast to the weak-motion, low magnitude far-field data of this study. These differences may give rise to differences in the expected behaviour of the resulting PGA. From the nonparametric description of peak accelerations above the Mexican subduction thrust, Anderson (1997) noted that the rate of decay of peak accelerations varied with respect to earthquake size. Accelerations from large earthquakes ($M > 6$) decreased more slowly with increasing distance from the site of energy release than accelerations from small earthquakes. Hadley and Helmberger (1980) also noted a decrease in the slope of the attenuation-distance relation with increasing magnitude. However, the rate of decrease of PGA is the same for Joyner and Boore (1981) as in the current study (Tables 4 and 6 and Figure 8) so it is not clear how important this effect may be.

Table 8. Distribution of data used in the calculation of strong-motion attenuation relations.

Model	Accel (g)			Distance (km)			Magnitude	
Joyner and Boore (1981)	0.004	to	0.810	1.2	to	370	M_w	= 5 to 7.7
Ambraseys and Bommer (1991)	0.001	to	0.99	1.0	to	313	M_S	= 2.6 to 7.3
Fukushima and Tanaka (1990)	0.002	to	1.2695	0.1	to	303	M_{JMA}	> 6
Molas and Yamazaki (1995)	> 0.001					< 200	M_{JMA}	= 4 to 8
Zhao *et al.* (1997)	0.110	to	0.98	11.00	to	573	M_w	= 5.1 to 7.4

Comparisons between the attenuation models derived in this study have been made with others in the literature, including the recent New Zealand model (Zhao et al., 1997), Japanese models (Fukushima and Tanaka, 1990; Molas and Yamazaki, 1995), the Western USA (Joyner and Boore, 1981) and Europe (Ambraseys and Bommer, 1991). As seen in Figures 9 and 10, the Japanese and Joyner and Boore (1981) models give the closest fit to the data. Similar to the findings of Zhao et al. (1997), the Fukushima and Tanaka (1990) model generally gives a better fit than does that of Molas and Yamazaki (1995). This is particularly true of data at distances >500 km. A comparison of Tables 4 and 6 shows that the anelastic attenuation rate of the CVRD is similar to that determined for Japan by Molas and Yamazaki (1995). Moreover, the fit of the data improves as the magnitude of the events increases (Figures 9 and 10).

Figures 9 and 10 also show comparisons between the Joyner and Boore (1981), Ambraseys and Bommer (1991) and Zhao et al. (1997) attenuation models. The Zhao et al. (1997) Model 5 is used for the comparison as it takes no account of focal mechanism or site conditions. However, the Zhao et al. (1997) relation does not include an anelastic attenuation term. From Tables 4 and 6, and Figure 8 we can see that the rates of anelastic attenuation found for this study are comparable to those of the tectonic regimes of Western USA (Joyner and Boore, 1981), as mentioned above. Once again we see that the model improves with increasing magnitude, with the best fit of the Joyner and Boore (1981) attenuation relation occurring at high magnitudes (Figure 10). This is contrary to the findings of Zhao et al. (1997) who noted that the difference between the Joyner and Boore (1981) and Ambraseys and Bommer (1991) models, in comparison with New Zealand strong motion data, decreases with decreasing magnitude. This is probably due to the differences in the magnitude range between Zhao et al. (1997) and the current study. Nonetheless, it is clear that the absolute level of attenuation predicted by the Ambraseys and Bommer (1991) and Zhao et al. (1997) models, as well as the Joyner and Boore (1981) model at low magnitudes, greatly differs from the data of this study. Moreover, Figures 8-10 indicate that the difference in absolute level is in some way related to the magnitude of the events.

Reasons to account for difference in absolute level

The observed differences in the absolute level, particularly at low magnitudes, between the strong motion attenuation relations and those of weak motion derived in this study may be the result of three factors: Differences between the strong motion and weak motion datasets, differences in magnitude scales and differences in frequency characteristics.

Near-source effects related to the fault and rupture geometry have an effect on near-field PGA values that have no bearing on far-field observations (Smith, 1995a,b). Most of the strong motion relations are derived using data at these distances, whereas the weak-motion attenuation relations presented here were obtained from data absent of near-field observations.

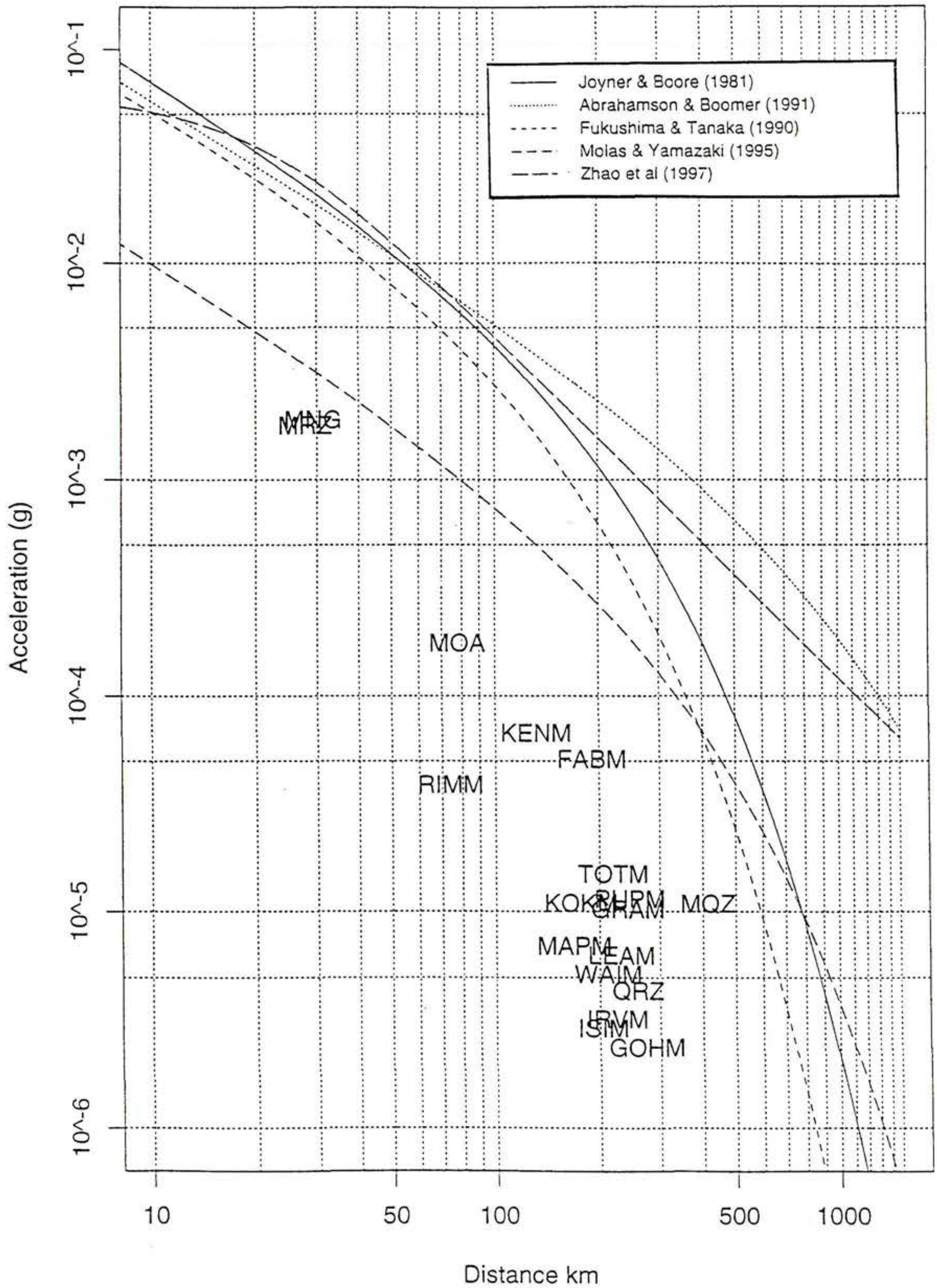

Figure 9. Comparison of strong-motion models with data from an ENIS event of M_L = 3.6 and depth = 27.4 km. Those of the Japanese data set are more comparable to the New Zealand weak motion than any of the others, including that of Zhao et al (1997).

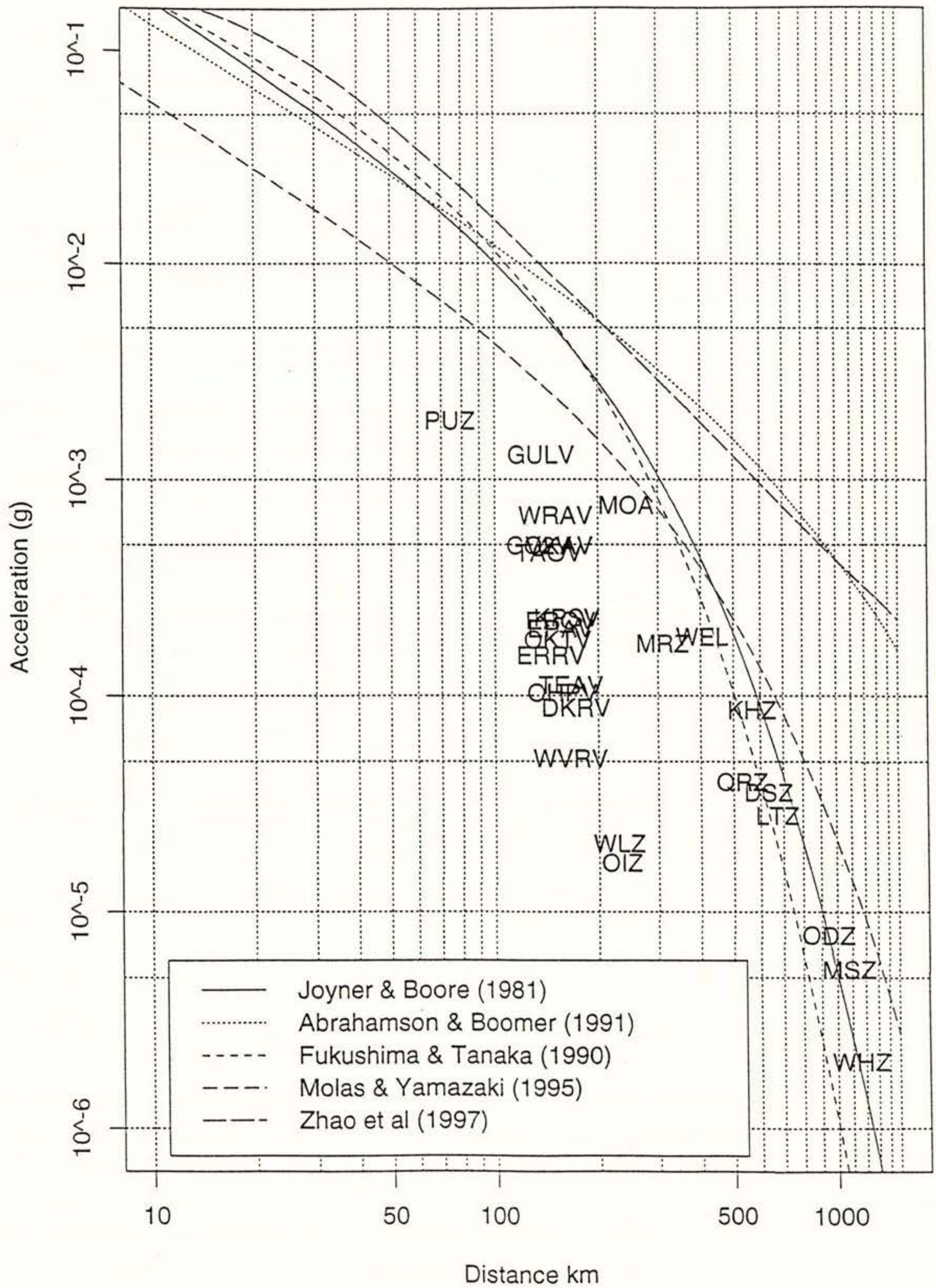

Figure 10. Comparison of strong-motion models with data from an ENIS event of M_L = 5.1 and depth = 33.0 km. Note the increasing improvement of the fit with increasing magnitude (compare with Figure 9).

Differences clearly exist between the strong- and weak-motion relations. Looking at Tables 4 and 6, one can see that the constant and magnitude terms of the weak-motion relations differ significantly from those of the strong-motion. One explanation is that the difference in absolute level of the two types of attenuation relations is due to a magnitude scale effect. Although M_L, which is used in this study, is comparable to the M_{JMA} scale (Frank Evison, personal communication), this is not true of M_s and M_w over all magnitude ranges. $M_L < M_S$ for $M_S > 6$ and $M_L > M_S$ for $M_S < 6$ (Kanamori, 1983, Dowrick, 1991a). This clearly suggests that there may be discrepancies resulting from differences in the magnitude scales used.

To investigate this further, three strong motion events for which both M_L and M_S values were available were analysed. These three earthquakes were located within the North Island of New Zealand (Table 2). The Joyner and Boore (1981) regression model and method were used to derive expressions for the attenuation described by these three events. Two expressions were regressed for; one using M_S values of magnitude, the other using M_L values. The results of this investigation are shown in Table 9. There is a distinct difference in the value of the constant and magnitude terms due to the two magnitude scales. Those derived using the M_S values are similar to those of Joyner and Boore (1981) and Ambraseys and Bommer (1991), while the M_L regression coefficients are similar to those determined by the larger data set (eg. Table 6). However, as seen from Figure 11, the two relations predict a level of PGA which is almost the same. The two regressions predict the same acceleration at M=6.5. At lower magnitudes. M_S values must be much smaller than M_L values for the regression to predict the same acceleration (Table 9). Thus in the comparison of the M_S attenuation relations to the M_L regressions calculated here (Figures 8-10), the M_S derived curves always lie above the M_L curves. This difference in magnitude scales should not affect the anelastic attenuation term since the two stage regression determines the magnitude effect separately.

Table 9. Effect of Magnitude scale on the attenuation relations derived from three strong motion events.

Mag Scale	Attenuation relation
M_L	log_{10} A = -5.2945 + 0.7957 M - log_{10} R - 0.00108 R
M_S	log_{10} A = -1.4321 + 0.2173 M - log_{10} R - 0.00108 R

The third possible explanation for the difference in absolute level, is the difference in frequency characteristics between strong- and weak-motion. Consider the source model of Brune (1970) which consists of a simple circular fault of radius r that ruptures over its whole area at the same time. The idealised amplitude spectrum of ground motion acceleration for shear waves from this source is shown in Figure 12. The corner frequency f_c marks the change in the spectrum from an increasing level

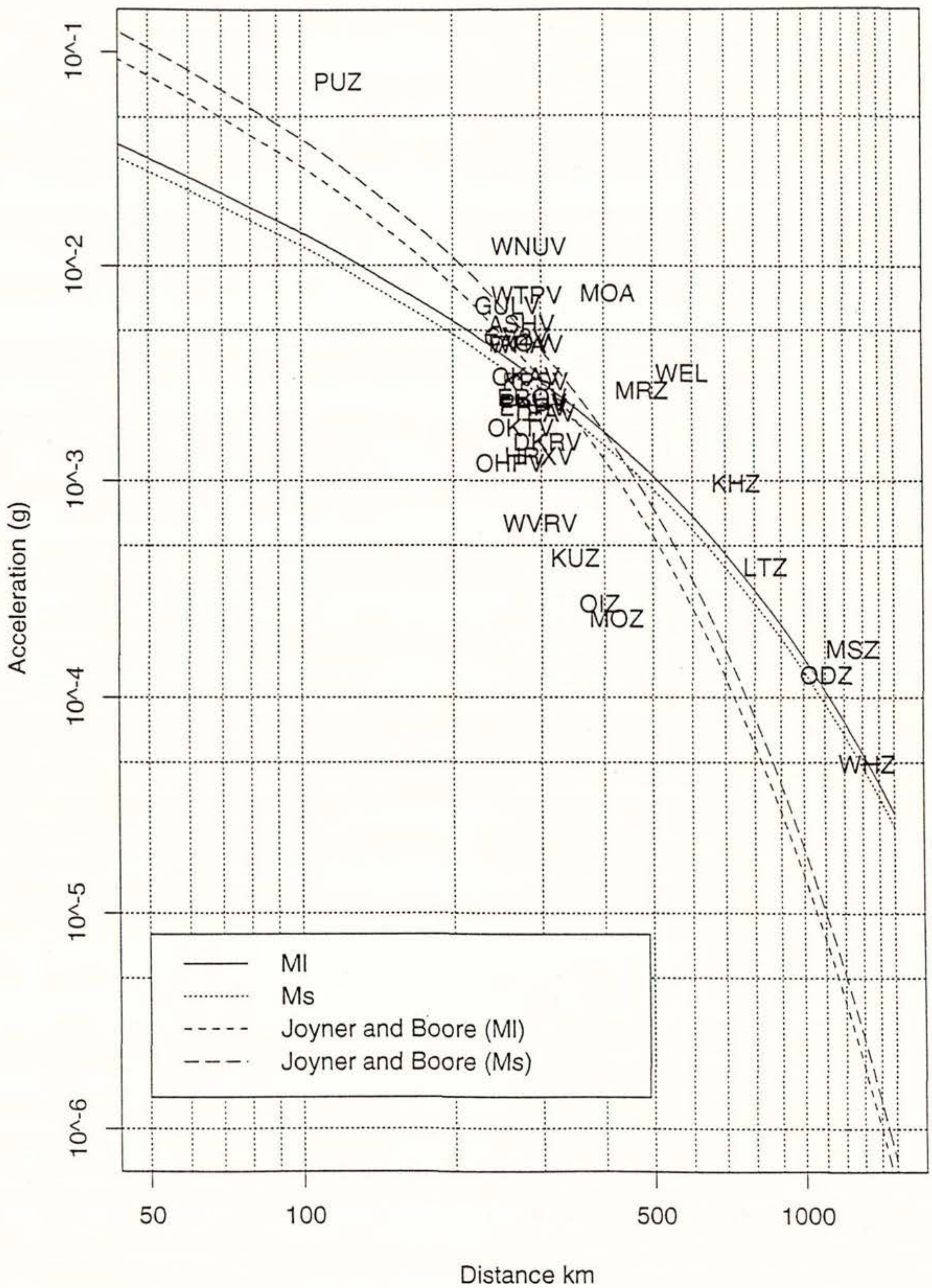

Figure 11. M_L and M_S regressions for three strong-motion events listed in Table 9 are plotted for the Feb 5 1994 event. The Joyner and Boore (1981) attenuation relation using the respective magnitude ($M_L = 6.98$, $M_S = 7.5$) values are also plotted for comparison.

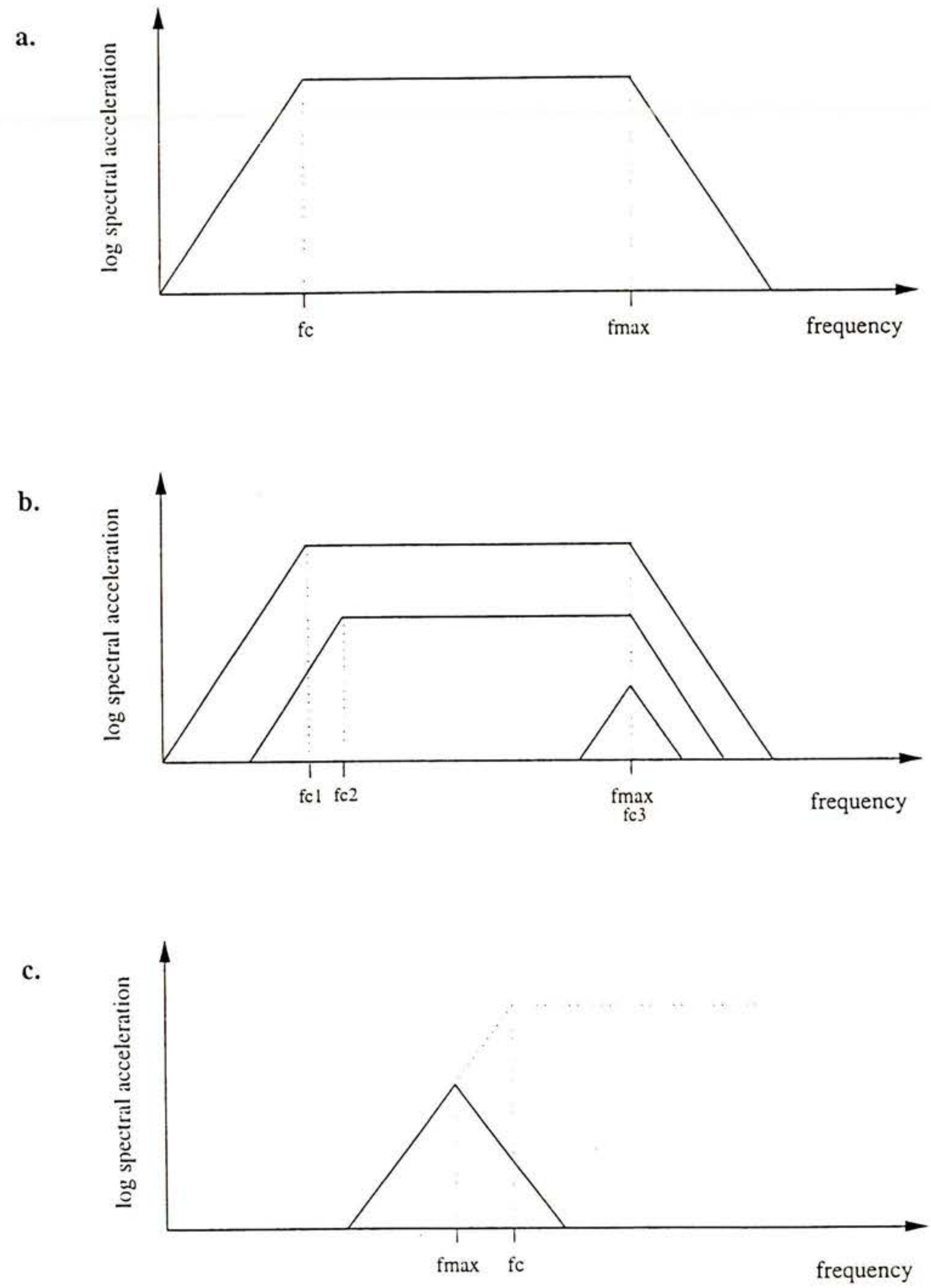

Figure 12. Idealised Fourier amplitude acceleration spectrum showing the relation between f_c and $f_{\max}$. Figure a. shows the general characteristics of the acceleration spectrum. f_c marks the frequency at which the spectral level becomes constant. At a higher frequency, $f_{\max}$, the spectral amplitude decays rapidly. Assuming $f_{\max}$ is a property of local site conditions, as f_c increases with decreasing magnitude, $f_{\max}$ remains constant (Figure b.). A frequency will be reached where $f_c = f_{\max}$ as illustrated in Figure b. If f_c continues to increase, the energy will continue to peak around $f_{\max}$ (Figure c.). However, the "true" level of the spectrum will be that at f_c. Thus the amplitude observed will be less than that expected for the given magnitude.

of acceleration to a constant level and increases with decreasing earthquake size. $f_{\max}$ describes the observed frequency at which an exponential decay of the acceleration frequency spectra initiates and is considered to be a site effect (Hanks, 1982; Papageoriou, 1988), not a source effect (Papageoriou and Aki, 1983), particularly considering the high frequencies which are visible in deep borehole data (Abercrombie, 1995).

The combination of these two effects could result in a faster decrease in maximum spectral acceleration for small earthquakes than for large earthquakes. Assuming $f_{\max}$ remains constant at a particular site, as f_c continues to increase, a frequency at which $f_c = f_{\max}$ will be reached (Figure 12b). As the earthquake size continues to drop, the "true" f_c exceeds the value of $f_{\max}$ (Figure 12c). However the maximum spectral accelerations observed will be that for which $f_c = f_{\max}$. This is lower than what would be expected, as shown by the dotted lines in Figure 12c. Thus the observed PGA of the motion is less than that expected for the magnitude of the event. Abercrombie (1995) noted that for events as small as $M_L = -1$, that were recorded at a depth of 2.5 km down a borehole, f_c continues to increase, ie $f_{\max}$ does not become a factor. As these events were recorded at depth, the frequency content was not effected by near-surface attenuation. Site-dependent limiting corner frequencies for small earthquakes have been noted by Frankel (1982). The possible overlap of f_c and $f_{\max}$ does not appear to be a major factor in the weak motion database as the peaked shape in Figure 12c is not evident for the low magnitude events that have been examined (Figure 13).

One or more of these three effects may have contributed to the difference between the strong motion relations and those of the weak-motion. Though the rate of attenuation of Ambraseys and Bommer (1991) is slightly different from those of the weak motion, the weak-motion rates are similar to Joyner and Boore (1981) suggesting that anelastic attenuation effects are not the cause. Moreover, the difference between the absolute level of the Joyner and Boore (1981) and weak motion relations increases with decreasing magnitude, as illustrated by Figures 8, 10, and 11. This suggests that the effect is most likely to be due to a difference in the M_L and M_S magnitude scales.

Consideration of wave propagation

Attenuation relations describe the smooth decrease of ground motion with distance. However, these relations may require a more complex form to account for wave propagation through the crust. Many strong-motion studies have noted that at mid-field distances, amplitudes become constant in value and there appears to be an absence of geometric spreading. These large amplifications have been determined to be the result of post-critical reflections from either mid-crustal discontinuities (Atkinson, 1995), the subducting slab (Atkinson, 1995), or the base of the crust (eg. Atkinson and Mereu, 1992). These reflections influence attenuation values at an average distance of about 50-150 km (eg. Mori and Helmberger, 1996). The degree at which these reflections effect the observed ground-motion depends greatly on the local geological and velocity structure (Burger et al., 1987; Mori and Helmberger, 1996), as

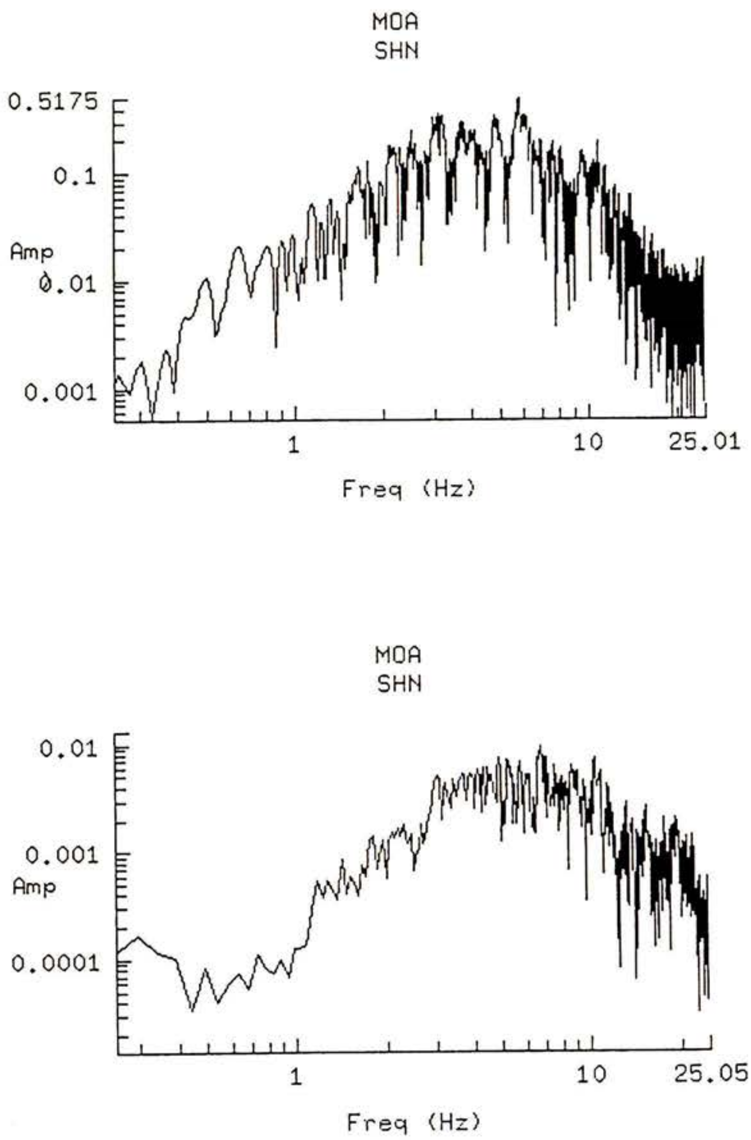

Figure 13. Acceleration spectra for station MOA for earthquakes of M_L 5.3 (top) and M_L 3.7 (bottom). Note that the high frequency decay is similar for the two earthquakes and appears to begin above the corner frequency (about 3 Hz for the smaller event).

well as focal depth (Atkinson, 1995; Somerville and Yoshimura, 1990). There should thus be a transition in the attenuation model between ground-motion dominated by direct arrivals at near-field distances to an interval at greater distances dominated by post-critical reflections (Burger et al., 1987).

An interval of constant amplitude due to post-critical reflections from crustal discontinuities were not visually observed from the data of this study. This is due to insufficient data at distances of 50-150 km and/or to the fact that the data were not at sufficiently shallow depths. Simple ray tracing across the North Island show that most reflections, including those from the Moho occur at distances of about 50-170 km. Most direct arrivals occur at distances less than 100 km, though shallow seismic sources transmit direct rays which extend to distances of the order of 100-200 km. The ray tracing indicates that the arrivals of this study are dominated by refractions from lower layers travelling in a north - south direction.

Similarly, the boundary of the highly attenuating material of the Central Volcanic Region cannot be determined because of the lack of closely spaced station distribution across the bounding regions. In order to determine the effects of direct and post-critical reflections on attenuation patterns, data across the whole distance spectrum is required.

Azimuthal Dependence

The amplitude, attenuation rate and spectral response of peak ground accelerations have been found to be azimuthally dependent in other regions (Campbell, 1991; Campbell and Bozorgnia, 1994). Factors influencing this dependence include source and path effects. Seismic sources lack spherical symmetry, and thus the radiation pattern plays an important role in the azimuthal variation of PGA, particularly in the near field. Ray paths parallel to the geological structure of a region, the geological "grain", in general experience less attenuation, while ray paths orientated perpendicular to structures, such as fault zones, are attenuated to a greater extent (Campbell, 1991).

The azimuthal variation of PGA has not been investigated for New Zealand earthquakes, though the azimuthal variation of isoseismals has been studied (Kozuch et al., 1996; Smith, 1978). The procedure of Kozuch et al. (1996), designed to quantify the azimuthal variation in a sparse data set, has been adopted in this study to examine the azimuthal dependence of PGA attenuation. The ENID, ENIS, CVRD, and CVRS data set were defined as in the previous section. An attempt was made to divide the Eastern North Island Deep and Shallow regions into north and south sections, but there were insufficient data for the separation.

The data for each region were divided into bins based on magnitude and acceleration values (Table 10). The magnitude and acceleration bins were combined to produce a total of 20 data bins for each region. The assumption has been made that all earthquakes within a specific region and bin produce azimuthally similar attenuation patterns (Figure 14), ie. the effect of source mechanisms has been ignored. For each earthquake-station pair, the distance and azimuth were used to project the origin

Table 10. Criteria for binning data for analysis of azimuthal dependence with respect to acceleration and magnitude.

Acceleration (g)						
A1	=	<	0.000001			
A2	=	≥	0.00001	and	<	0.0001
A3	=	≥	0.0001	and	<	0.0001
A4	=	≥	0.001			
Magnitude M_L						
M1	=	≥	3.0	and	<	3.5
M2	=	≥	3.5	and	<	4.0
M3	=	≥	4.0	and	<	4.5
M4	=	≥	4.5	and	<	5.0
M5	=	≥	3.5			

Table 11. Number of data per bin used for azimuthal analysis.

Bin	Region	Number of data points
A2.M4	CVRS	37
A1.M2	CVRD	50
A1.M3	CVRD	188
A2.M3	CVRD	282
A2.M3	ENIS	86
A2.M4	ENIS	70
A2.M3	ENID	101
A3.M2	ENID	42
A3.M3	ENID	57

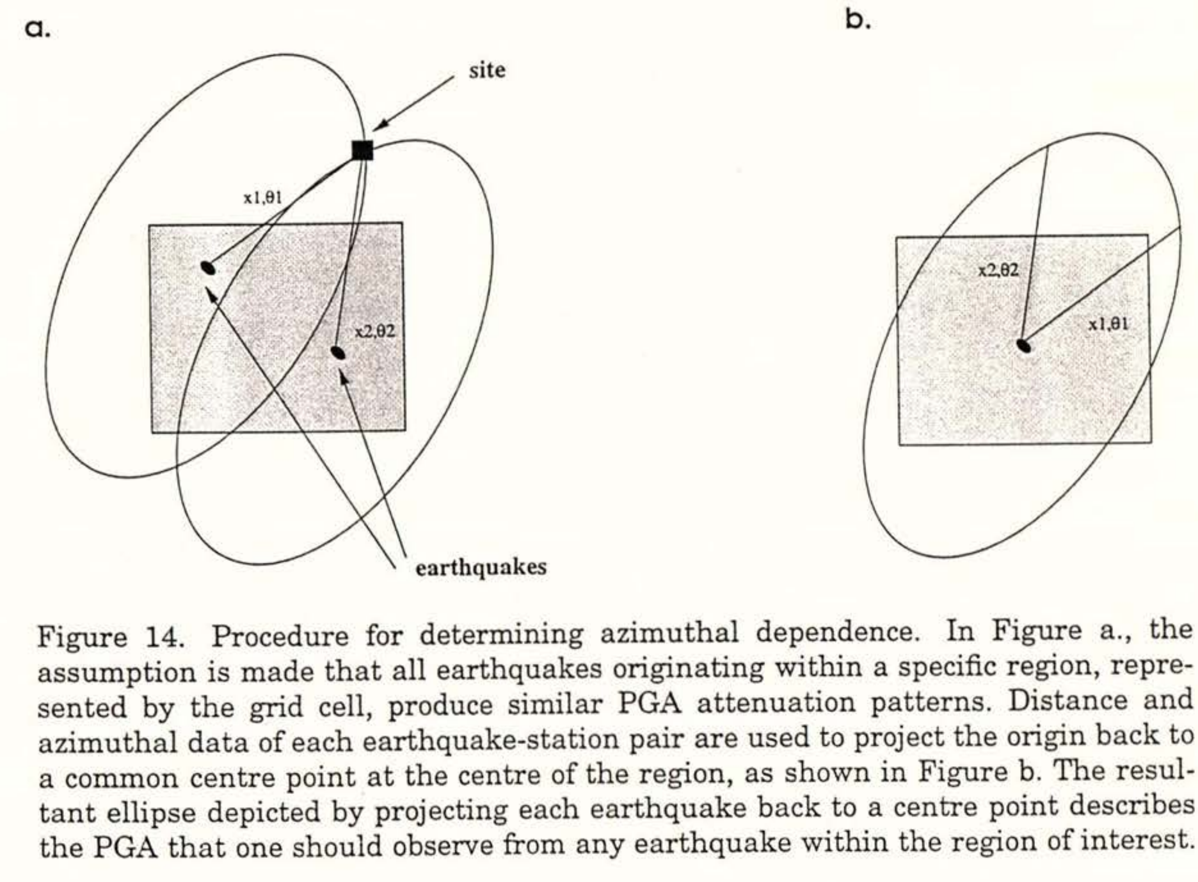

Figure 14. Procedure for determining azimuthal dependence. In Figure a., the assumption is made that all earthquakes originating within a specific region, represented by the grid cell, produce similar PGA attenuation patterns. Distance and azimuthal data of each earthquake-station pair are used to project the origin back to a common centre point at the centre of the region, as shown in Figure b. The resultant ellipse depicted by projecting each earthquake back to a centre point describes the PGA that one should observe from any earthquake within the region of interest.

back to a common point at the centre of the region, Figure 14b. An ellipse was then fitted to the data.

If the area of each region of interest were decreased, the variation of the orientation and shape of the ellipses describing the attenuation within each bin might also decrease, since within a smaller area there are fewer fault orientations. However, in order to decrease the size of the regions considered in this study, additional data would be required to obtain plausible results.

For each region, a plot of the data projected back to the centre of the region was made. To overcome the bias due to an azimuthally uneven station distribution, the data were truncated at radial distances so that data were approximately evenly distributed at all azimuths. The truncation values were 700 km for the CVRD, 625 km for the CVRS, 300km for the ENID region, and 375 km for the ENIS region.

To maximise the use of limited data, data points within a single bin were projected onto the x axis (Kozuch et al., 1996)(Figure 15). They were then "folded" onto the positive x quadrant. The axes were rotated by increments, in this case 5°, until 180° had been completed. After each rotation, the process of mapping data points onto the new positive x axis was repeated. Because of the symmetry of an ellipse, rotation through 180° was all that was required. The combined data were in this way grouped according to the distance along the x axis and the corresponding degree of rotation. The orientation of the minimum and maximum axes of the ellipse described by the data was then determined from the resulting plot (Figure 16). To aid the determination of the orientation and shape of the ellipse, the median value of the PGA at each azimuthal increment was overlaid onto the plots (Figure 16). A smoothed curve was then fitted to the median points. These curves were used to determine the position of the axes. The procedure was first tested using a known ellipse to determine the limits of the technique. It was found that the data must be evenly distributed over two adjacent quadrants to accurately describe an ellipse and that while the major and minor axes of the distribution are correctly determined, the ratio of the length of the major and minor axes does not give the true ellipticity for data that includes random scatter.

Although all of the 20 data bins for each region were considered, all but 9 were discarded because the bins either contained too few data, or the data were not evenly distributed over two adjacent quadrants. The Central Volcanic Region in particular had a very sparse data set. Table 11 lists the number of data points in each of the bins that contain sufficient data. The major and minor axes of these bins are shown in Figure 17. The figure shows that there is a distinct azimuthal dependence of PGA attenuation for these bins.

The orientation of the minor axes (the direction of greatest attenuation) for all bins in the Central Volcanic Deep Region is about 115-125° from North. For the bin with major and minor axes perpendicular to each other, the major axis is orientated at about 35°. For the two bins where the major and minor axes are not orthogonal, the major axis is orientated at about 55°. Such a distribution, where the major and minor axes are not perpendicular, may occur because earthquakes within this region

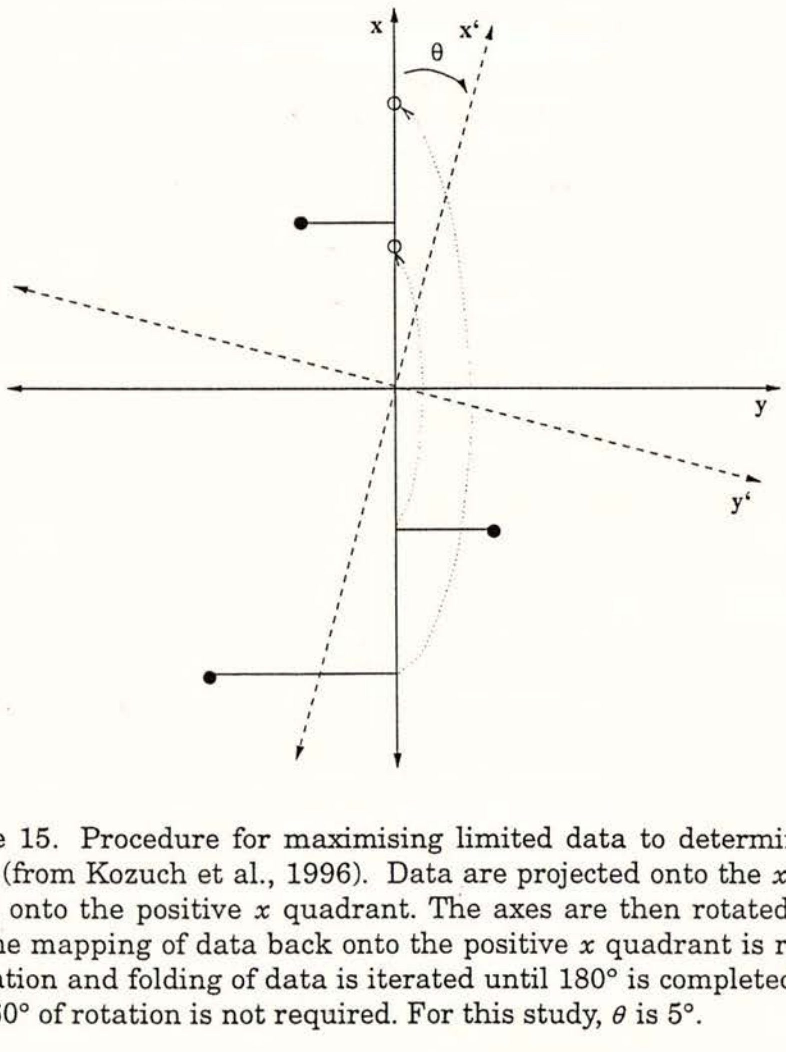

Figure 15. Procedure for maximising limited data to determine azimuthal dependence (from Kozuch et al., 1996). Data are projected onto the x axis. They are then folded onto the positive x quadrant. The axes are then rotated by an increment, θ, and the mapping of data back onto the positive x quadrant is repeated. The process of rotation and folding of data is iterated until 180° is completed. Because of symmetry, 360° of rotation is not required. For this study, θ is 5°.

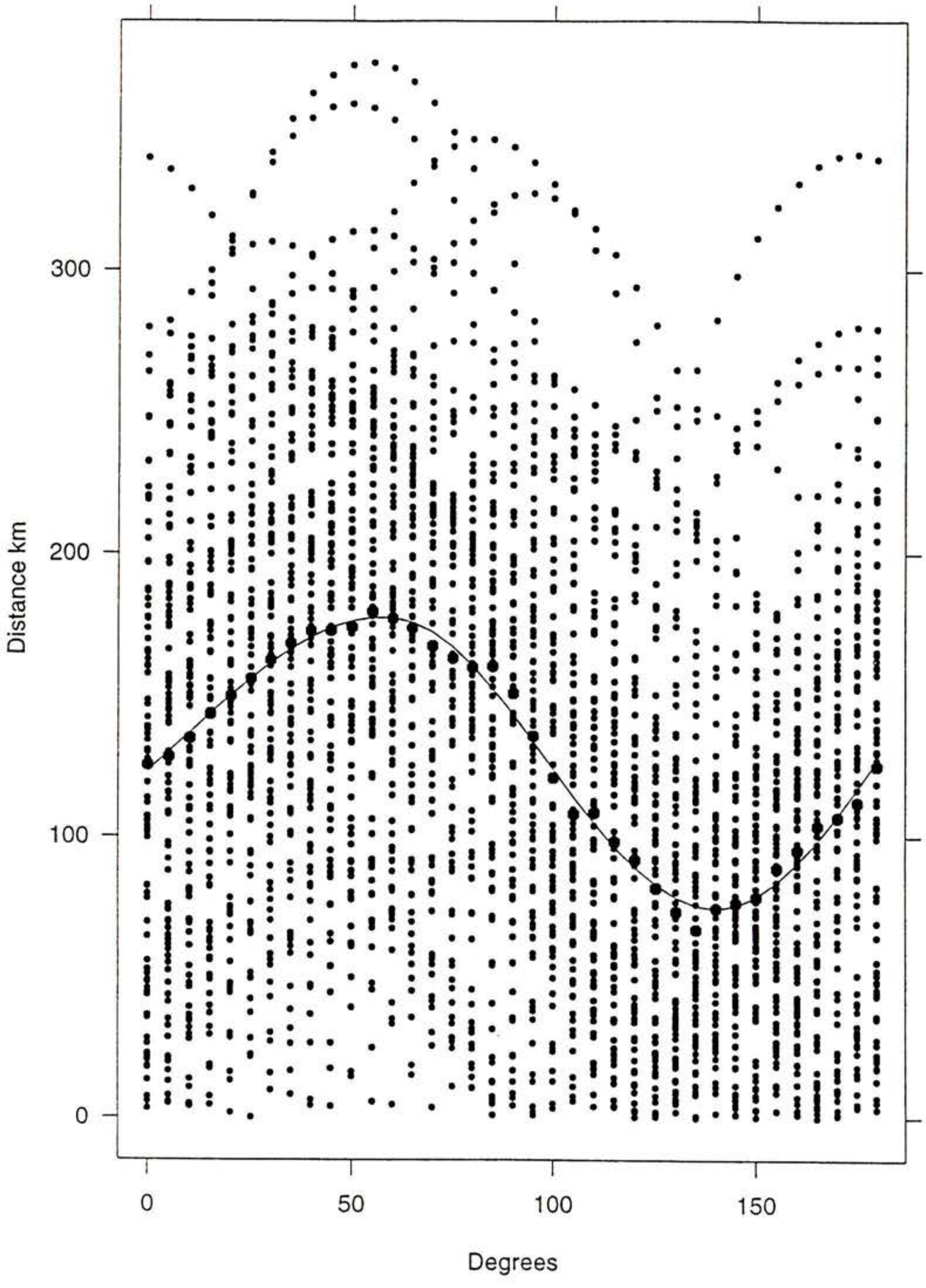

Figure 16. Plot of data from the ENIS A2M3 data bin. Data obtained through rotating the axes and mapping data points onto the positive x axis are plotted against the rotation increment. The median data value for each increment of rotation has been superimposed on the plot (large dots) as well as a smoothed fit to these points (solid line). Both the fitted curve and the median points were used to estimate the major and minor axes and their orientation. In this example, the major axis is oriented at 50° with a length of 180 km. The minor axis is oriented 90° to the major axis at 140° with a length of 70 km.

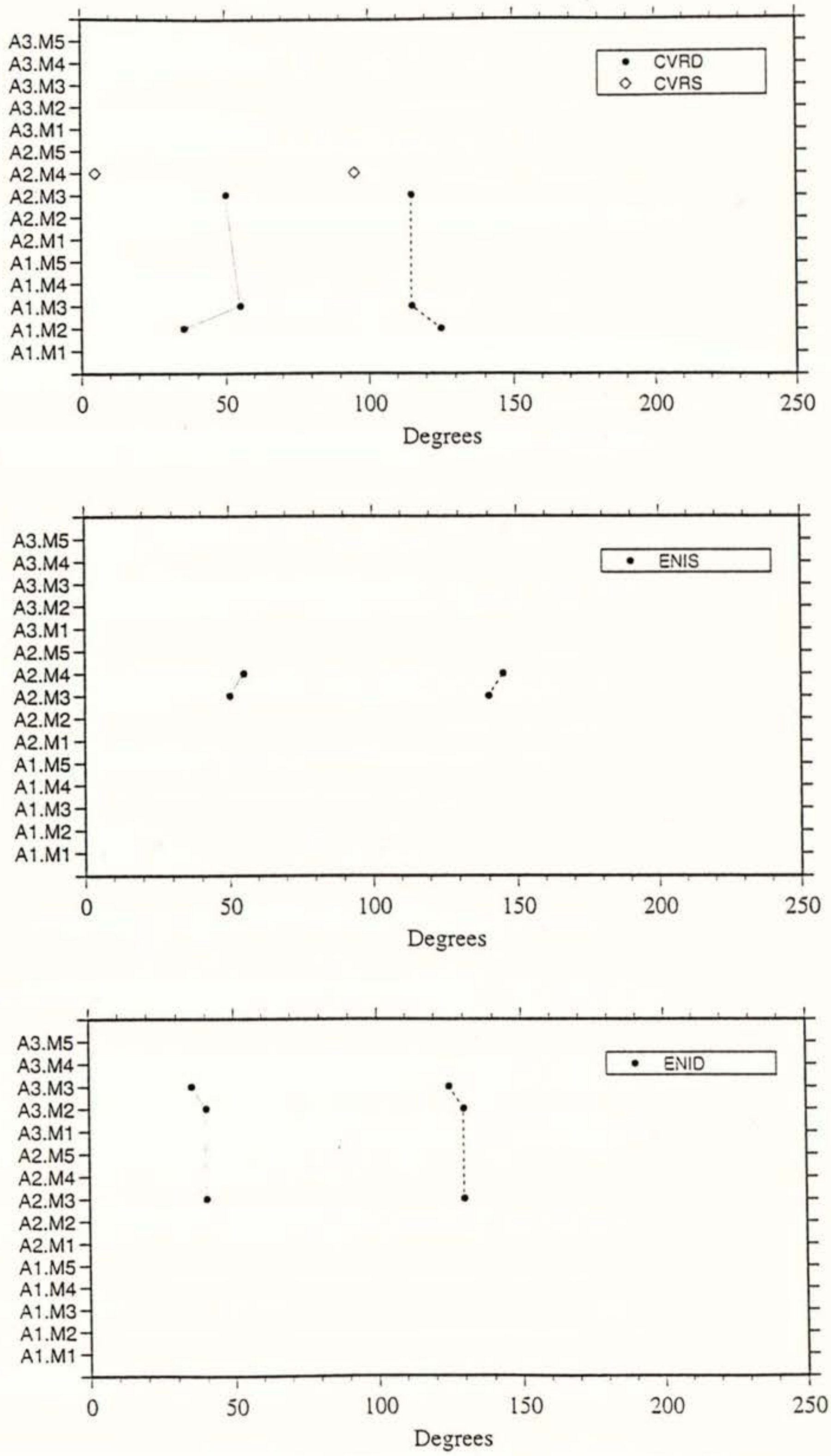

Figure 17. Plot of orientation of major (dotted line) and minor (dashed line) axes of ellipses determined for the CVRD and CVRS (top) ENIS (middle), and ENID (bottom) regions. Note that the CVRD A1M3 and A2M3 axes are not perpendicular to each other.

originate in the subducting slab. Ray paths travelling longer distances through the slab will experience less attenuation than those travelling through the mantle and the orientation of this low attenuation path is different from the low attenuation direction in the crust.

Within the ENIS region, the major axes are oriented at 35-60° while the minor axes are orientated at about 125-150° (Figure 17). This differs slightly from those of the ENID region. Ellipses of the ENID region have major axes orientated at 30-40° and minor axes orientated at 120-130°. These differences are probably not significant.

The orientation of the major axis of the one bin in the CVRS is 5°, while the minor axis is oriented at 95°. Thus there appears to be a difference in the azimuthal variation of attenuation for waves originating in the CVRS compared to all the other regions.

It is unclear whether the small differences between the azimuthal dependence of the Eastern North Island and deep Central Volcanic Region are due to tectonic differences or are simply due to the sparse data. The orientation of the minor axes of the ENID and CVRD are comparable, while slight differences in the orientation of the major axes of the CVRD and ENID may be due to the fact that earthquakes of the CVRD originate deeper in the subducting slab.

The length of the major and minor axes in Figure 16 cannot be used to determine the true variation of attenuation with azimuth. The actual ratio of major to minor axis length as estimated from the data bins (Figure 18), varies from barely over 1 to about 2.5. A more precise way of quantifying the distribution is needed along with a higher density of data to determine the true level of the azimuthal variation in attenuation.

The orientation of the major axes within the Eastern North Island regions agree with the strike of the Hikurangi subduction zone. This is consistent with the findings of Kozuch et al. (1996) and Marson (1997). Marson (1997) noted that the fast direction of S phases recorded at Karori, New Zealand, parallelled the strike of the subduction complex as well as the local geological structure. Differences exist, however, between the azimuthal dependence of attenuation determined in this study and that of Kozuch et al. (1996) for the CVR. Kozuch et al. (1996) observed no distinct azimuthal dependence within the CVR, whereas such a dependence was found in the current study. From this study it appears that both the highly attenuating material of the Central Volcanic Region and subducting Pacific Plate have a directional influence on PGA attenuation and that these azimuthal influences may differ from those of the Eastern North Island.

Conclusions

Regression analysis of peak ground accelerations of weak motion data has permitted differences in attenuation rates between the Eastern North Island and Central Volcanic Regions to be quantified. The attenuation relations were based on the source

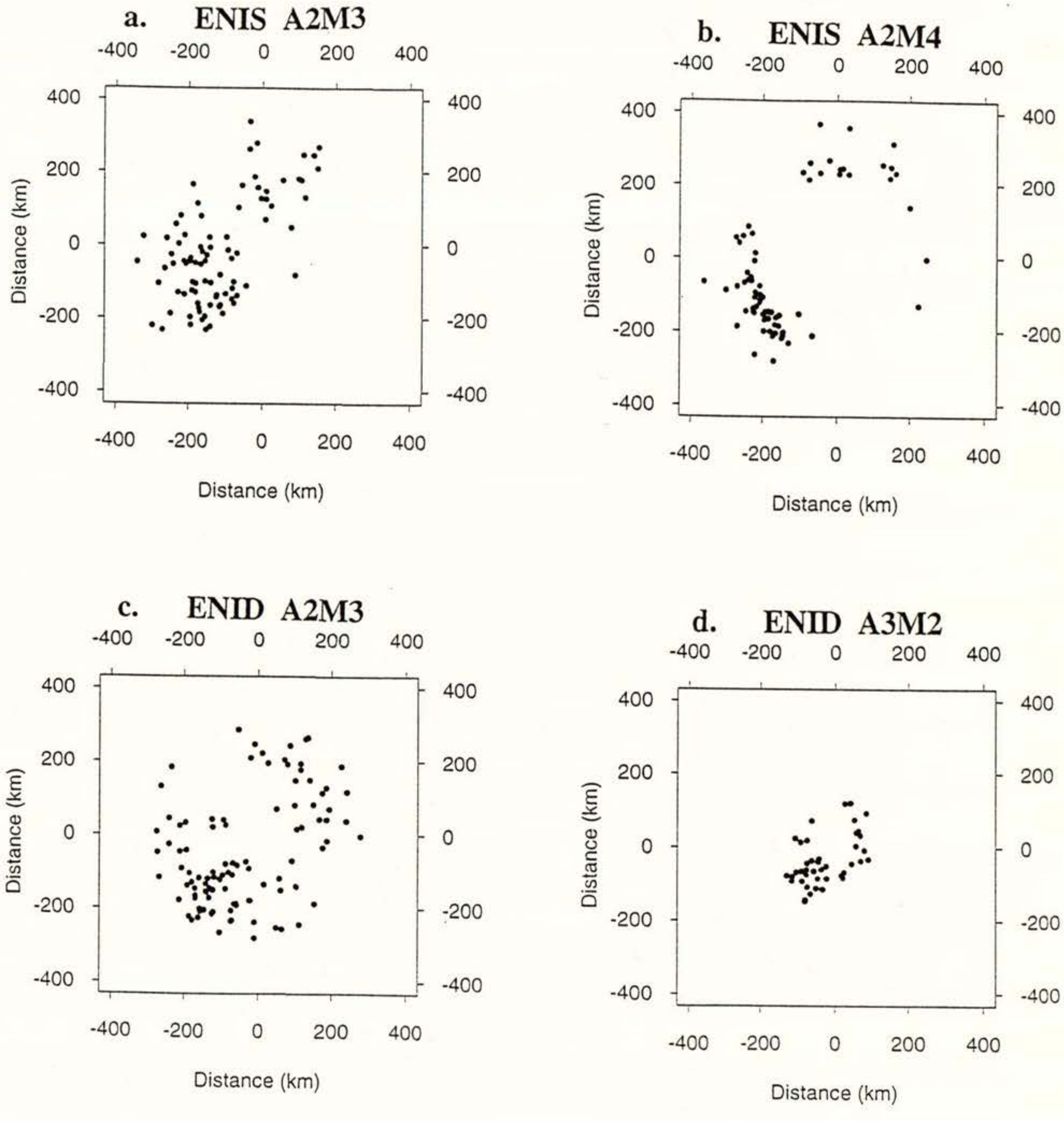

Figure 18. Distance and azimuthal distribution of four acceleration data bins: a. ENIS A2M3, b. ENIS A2M4, c. ENID A2M3, d. ENID A3M2.

regions of the earthquakes. As expected it has been found that seismic waves which travel through the CVR are more attenuated than those through the subducting slab of the Pacific Plate and the overlying crust of the Australian Plate. The anelastic attenuation rate of seismic waves from deep earthquakes travelling exclusively through the CVR was found to be -0.007 g/km, while the rate for deep earthquakes in the Eastern North Island region was of the order of -0.003 g/km. Shallow earthquakes within the CVR experience an even greater rate of anelastic attenuation of -0.067 g/km. The lowest attenuation was determined for deep earthquakes in the CVR that were recorded in the Eastern North Island region. The seismic waves for these events spent a greater proportion of their time travelling up the subducting slab, which implies a lower attenuation in the slab.

It was hoped that the regression analysis would define the boundary between the attenuating zone of the CVR and that of the surrounding regions. However, due to the lack of a closely spaced station distribution across the bounding area, this was not achieved. Since the beginning of this project, significantly more 3-component data have been collected by the NZNSN, so it may soon be possible to define the boundary. Additionally this project concentrated on events with large numbers of recording stations (an average of 17), so it may be possible to improve the coverage by including less-well-recorded events.

On comparison with strong motion relations, it was found that the weak motion relations had greatest similarities with Japanese models (Fukushima and Tanaka, 1990; Molas and Yamazaki, 1995), particularly at high magnitudes. The attenuation rate for travel paths from deep earthquakes in the CVR to sites outside the region agree with that of Molas and Yamazaki (1995). Attenuation models from Europe and New Zealand were found to significantly overpredict the weak motion. The rate of attenuation of the Eastern North Island weak motion data is comparable to the Joyner and Boore (1981) model for Western US, absolute values of the relation agree only at high magnitudes. At low magnitudes the absolute level of the Joyner and Boore (1981) attenuation model also greatly overpredicts the weak motion.

Three factors were considered in determining the cause of this overestimation at low magnitudes: 1. the difference in characteristics of PGA between near- and far-field and weak- and strong-motion data. 2. differences between the magnitude scales adopted. 3. differences in the frequency level. We conclude that the primary effect is due to the difference in the M_L magnitude scale used for the weak motion models and the M_S scale used for the strong motion models. The determination of M_S values for some of the small earthquakes used in this study could help resolve this issue. However the difference in magnitude scale should not effect the anelastic attenuation term. Thus the weak motion results presented here should be relevant to strong-motion relations.

Azimuthal dependence of PGA determined within the Eastern North Island region corresponds to that determined using isoseismals (Kozuch et al, 1997), with the major axis oriented parallel to the strike of the subducting slab. An azimuthal dependence was also found in the CVR contrary to the isoseismal study. Within the CVRS, preferred directions appear to be influenced by the more northerly trending structures of the region(Grindley and Hull, 1986). It was also found that the major and minor axes of "ellipses" describing PGA attenuation in the CVRD may not be perpendicular to each other. This may be due to the differences in preferred directions in the subducting slab and the overlying crust. The lengths of the axes could not be accurately determined using the method applied. Further investigation with a larger data set and a more precise method is required to do so. The azimuthal variations of the baseline attenuation patterns within each region may have implications on the attenuation relations developed here.

Acknowledgments

We are very grateful for the use of data from the Institute of Geological and Nuclear Sciences earthquake catalogue. Much of the data used for this study was recorded by the National Seismograph Network. We also appreciate the many people at IGNS responsible for the collection of the additional data collected via temporary networks. These people include Tony Hurst, and especially the project leaders Martin Reyners, for the Marlborough and Eastern North Island deployments, and Hugh Bibby, for the TVZ deployment. Brian Dawkins provided significant statistical insight, and important comments on the manuscript were provided by Euan Smith. We also wish to thank the Earthquake Commission for their financial support of this project, which is the basis of Aasha Pancha's Masters thesis, and for John Taber's EQC Fellowship.

References

ABERCROMBIE, R. (1995), Earthquake source scaling relationships from -1 to 5 M_L using seismograms recorded at 2.5-km depth, *J. Geophys. Res.* **100**(B12): 24,015–24,036.

AMBRASEYS, N. N. AND BOMMER, J. J. (1991), The attenuation of ground accelerations in Europe, *Earthquake Eng. and Str. Dyn.* **20**: 1179–1202.

ANDERSON, J. G. (1997), Nonparametric Description of Peak Acceleration Above a Subduction Thrust, *Seis. Res. Letters* **68**(1): 86–93.

ATKINSON, G. M. (1995), Attenuation and Source Parameters of Earthquakes in the Cascadia Region, *Bull. Seism. Soc. Am.* **85**(5): 1327–1342.

ATKINSON, G. M. AND MEREU, R. F. (1992), The Shape of Ground Motion Attenuation Curves in Southeastern Canada, *Bull. Seism. Soc. Am.* **82**(3): 2014–2031.

BOLT, B. A. AND ABRAHAMSON, N. A. (1982), New Attenuation Relations for Peak and Expected Accelerations of Strong Ground Motion, *Bull. Seism. Soc. Am.* **72**(6): 2307–2321.

BROOK, R. J. AND ARNOLD, G. C. (1985), *Applied regression analysis and experimental design*, Marcel Dekker Inc.

BRUNE, J. N. (1970), Tectonic stress and the spectra of seismic shear waves from earthquakes, *J. Geophys. Res.* **75**: 49997–1009.

BURGER, R. W., ANMD J. S. BARKER AMD R. B. HERMANN, P. G. S. AND HELMBERGER, D. V. (1987), The Effect of Crustal Structure on Strong Ground Motion Attenuation Relations in Eastern North America, *Bull. Seism. Soc. Am.* **77**(2): 420–439.

CAMPBELL, K. W. (1991), An Empirical Analysis of Peak Horizontal Acceleration for the Loma Prieta, California, Earthquake of 18 October 1989, *Bull. Seism. Soc. Am.* **81**(5): 1838–1858.

CAMPBELL, K. W. AND BOZORGNIA, Y. (1994), Emperical Analysis of Strong Ground Motion from the 1992 Landers, California, Earthquake, *Bull. Seism. Soc. Am.* **84**(3).

CHAMBERS, J. M. AND HASTIE, T. J. (Eds) (1992), *Statistical models in S, Chapter 4 "Linear models"*, Wadsworth and Brooks/Cole.

DOWRICK, D. J. (1991a), Magnitude Reassessment of New Zealand Earthquakes, *Earthquake Eng. and Str. Dyn.* **20**: 557–596.

DOWRICK, D. J. (1991b), A Revision of Attenuation Relationships for Modified Mercalli Intensity in New Zealand Earthquakes, *Bull. N.Z. Natl. Soc. Earthquake Engineering* **24**(3): 210–224.

DOWRICK, D. J. AND SRITHARAN, S. (1993a), Attenuation of Peak Ground Accelerations in some recent New Zealand Earthquakes, *Bull. N.Z. Natl. Soc. Earthquake Engineering* **26**(1): 3–13.

DOWRICK, D. J. AND SRITHARAN, S. (1993b), Peak Ground Accelerations Recorded in the 1968 Inangahua Earthquake and some Attenuation Implications, *Bull. N.Z. Natl. Soc. Earthquake Engineering* **26**(3): 349–355.

DRAPER, N. R. AND SMITH, H. (1981), *Applied Regression Analysis*, 2 edn, Wiley and Sons, Inc.

FRANKEL, A. (1982), The effects of attenuation and site response on the spectra of microearthquakes in the northeastern Caribbean, *Bull. Seis. Soc. Am.* **72**: 1379–1402.

FUKUSHIMA, Y. AND TANAKA, T. (1990), A New Attenuation Relation for Peak Horizontal Acceleration of Strong Earthquake Ground Motion in Japan, *Bull. Seism. Soc. Am.* **80**(4): 757 – 783.

GLEDHILL, K. R., RANDALL, M. J. AND CHADWICH, M. P. (1991), The EARSS digital seismograph: system description and field trials, *Bull. Seism. Soc. Am.* **81**(4): 1380–1390.

GRINDLEY, G. W. AND HULL, A. G. (1986), Historical Taupo earthquakes and earth deformation, *R. Soc. N. Z. Bull.* **24**: 173–186.

HADLEY, D. M. AND HELMBERGER, D. V. (1980), Simulation of Strong Ground Motion, *Bull. Seism. Soc. Am* **70**(2): 617–630.

HAINES, A. J. (1981), A Local Magnitude Scale for New Zealand Earthquakes, *Bull. Seism. Soc. Am.* **71**(1): 275–294.

HANKS, T. C. (1982), f_{max}, *Bull. Seism. Soc. Am.* **72**(6): 1867–1879.

JOYNER, W. B. AND BOORE, D. M. (1981), Peak Horizontal Acceleration and Velocity from Strong-Motion Records Including Records from the 1979 Imperical Valley, California, Earthquake, *Bull. Seism. Soc. Am.* **71**(6): 2011–2038.

KANAMORI, H. (1983), Magnitude Scale and Quantification of Earthquakes, *Tectonophysics* **93**(3-4): 185–199.

KOZUCH, M. J. E., SMITH, E. AND VERE-JONES, D. (1996), Modeling New Zealand isoseismal shapes with a site-specific attenuation dependence (abstract), *EOS, Trans. AGU, supplement* **77**(46): F510.

MARSON, K. (1997), *Seismic Anisotropy in the Wellington Region: Shear-Wave Splitting Results*, Report 1997/02, Institute of Geophysics, Victoria University of Wellington.

MATUSCHKA, T. AND DAVIS, B. K. (1991), Derivation of an Attenuation Model in terms of Spectral Acceleration for New Zealand, *Pacific Conference on Earthquake Engineering*, pp. 123–134.

MCVERRY, G. H. (1986), Uncertainties in Attenuation Relations for New Zealand Seismic Hazard Analysis, *Bull. N.Z. Natl. Soc. Earthquake Engineering* **19**(1): 28–39.

MOLAS, G. L. AND YAMAZAKI, F. (1995), Attenuation of Earthquake Ground Motion in Japan Including Deep Focus Events, *Bull. Seism. Soc. Am.* **85**(5): 1343 – 1358.

MOONEY, H. M. (1970), Upper Mantel Inhomogeneity beneath New Zealand: Seismic Evidence, *J. Geophys. Res.* **75**(2): 285–309.

MORI, J. AND HELMBERGER, D. (1996), Large-Amplitude Moho Reflections *SmS* from Landers Aftershocks, Southern California, *Bull. Seism. Soc. Am.* **86**(6): 1845–1852.

PAPAGEORIOU, A. S. (1988), On two characteristic frequencies of acceleration spectra: Patch corner frequency and f_{max}, *Bull. Seism. Soc. Am.* **78**(2): 509–529.

Papageoriou, A. S. and Aki, K. (1983), A specific barrier model for the quantitative description of inhomogeneous faulting and the prediction of strong ground motion. Part II. Applications of the Model, *Bull. Seism. Soc. Am.* **73**(4): 953–978.

Satake, K. and Hashida, T. (1989), Three-Dimensional attenuation structure beneath North Island, New Zealand, *Tectonophysics* **159**: 181–194.

Smith, W. D. (1978), Spatial distribution of felt intensities for New Zealand earthquakes, *N.Z Journal of Geology and Geophysics* **21**(3): 293–311.

Smith, W. D. (1995a), A Development in the Modelling of Far-Field Intensities for New Zealand Earthquakes, *Bull. N.Z. Natl. Soc. Earthquake Engineering* **28**(3): 196–217.

Smith, W. D. (1995b), A Procedure for Modelling Near-Field Earthquake Intensities, *Bull. N.Z. Natl. Soc. Earthquake Engineering* **28**(3): 218–223.

Smith, W. D. and Berryman, K. R. (1983), Revised Estimates of Earthquake Hazrad in New Zealand, *Bull. N.Z. Natl. Soc. Earthquake Engineering* **16**(4): 259–272.

Somerville, P. and Yoshimura, J. (1990), The Influence of Critical Moho Reflections on Strong Ground Motions Recorded in San Francisco and Oakland During the 1989 Loma Prieta Earthquake, *Geophys. Res. Letters* **17**(8): 1203–1206.

Venables, W. N. and Ripley, B. D. (1994), *Modern applied statistics with S-plus*, Spring-Verlag. New York, Inc.

Weisberg, S. (1985), *Applied Linear Regression*, 2 edn, John Wiley and Sons.

Zhao, J. X., Dowrick, D. J. and McVerry, G. H. (1997), Attenuation of Peak Ground Acclerations in New Zealand Earthquakes, *Bull. N.Z. Nat Soc. for Earthquake Engineering* **3**(2): 133–158.

Appendix 1. List of events used for regressions.

depth	mag	long	lat	region
104.2	3.81	175.4072	-39.3449	CVRD
147.5	4.23	176.4071	-38.0354	CVRD
126.7	4.27	176.5614	-38.0816	CVRD
197.0	4.46	177.0349	-36.9520	CVRD
160.0	4.14	176.4041	-38.1087	CVRD
136.8	4.13	176.9548	-37.5868	CVRD
142.1	4.24	176.4951	-37.9145	CVRD
144.2	4.38	176.8483	-37.8577	CVRD
184.7	4.62	176.0669	-38.2033	CVRD
149.7	4.00	175.3048	-39.0049	CVRD
176.2	4.24	176.2289	-38.1409	CVRD
198.5	4.19	176.0691	-38.1425	CVRD
207.9	4.01	175.1840	-38.9186	CVRD
198.9	4.36	176.2184	-37.9791	CVRD
184.5	3.79	175.7648	-38.5461	CVRD
164.9	4.19	176.2845	-38.0937	CVRD
144.4	3.67	175.2461	-39.1197	CVRD
275.1	4.36	176.2796	-37.4708	CVRD
155.6	5.47	175.3802	-39.0414	CVRD
158.8	4.27	176.0984	-38.2533	CVRD
161.8	5.33	175.9689	-38.4298	CVRD
159.4	5.13	176.0217	-38.3474	CVRD
161.8	5.04	176.3843	-38.1422	CVRD
213.5	4.40	175.2147	-38.8334	CVRD
252.4	4.33	175.7725	-37.6196	CVRD
228.4	4.41	175.2632	-38.6322	CVRD
144.7	3.90	176.1801	-38.1198	CVRD
181.6	4.24	176.4066	-37.5754	CVRD
167.4	4.15	175.7275	-38.6733	CVRD
151.4	4.04	175.9259	-38.5385	CVRD
161.9	4.13	176.0516	-38.4566	CVRD
157.1	4.42	175.9847	-38.4217	CVRD
12.0	4.69	177.0170	-36.7088	CVRS
18.7	4.80	177.4673	-37.0557	CVRS
12.0	4.81	178.1960	-35.6855	CVRS
33.0	5.44	178.2905	-35.5966	CVRS
5.0	4.11	176.1868	-38.4510	CVRS
5.0	3.34	176.9963	-37.6554	CVRS
5.0	3.46	176.8915	-37.9165	CVRS
12.0	4.62	177.0915	-36.6283	CVRS
33.0	4.03	178.5508	-36.0697	CVRS
12.0	3.61	176.2105	-38.4191	CVRS
12.0	4.02	177.9638	-36.6182	CVRS
5.0	3.41	176.6928	-38.1891	CVRS
33.0	3.77	178.3570	-36.0165	CVRS
5.0	3.49	176.4177	-38.2485	CVRS
5.0	3.90	175.3358	-39.2160	CVRS
5.0	3.64	175.3640	-39.2381	CVRS
5.0	3.63	175.3620	-39.2343	CVRS
5.0	4.28	177.4103	-37.2752	CVRS
12.0	4.47	177.4863	-37.1253	CVRS
5.0	3.61	175.7265	-38.8632	CVRS
5.0	3.92	175.3697	-39.2387	CVRS
12.0	3.88	175.4168	-39.1928	CVRS
5.0	4.78	175.3180	-39.2587	CVRS
12.0	4.24	177.3934	-37.1795	CVRS
12.0	4.41	177.3998	-37.2247	CVRS

depth	mag	long	lat	region
60.2	3.53	177.3388	-37.6477	ENID
45.9	3.71	177.2646	-38.0078	ENID
51.7	3.37	177.8561	-38.5057	ENID
57.7	3.33	177.7139	-38.3704	ENID
67.6	4.08	177.2650	-37.7277	ENID
55.1	3.65	177.3971	-38.3212	ENID
82.2	3.87	176.2794	-39.1739	ENID
33.6	4.43	177.5905	-37.8270	ENID
60.0	3.91	176.0109	-39.3207	ENID
89.5	3.45	174.8482	-40.2410	ENID
52.9	4.19	175.9148	-39.4289	ENID
59.6	3.68	174.2211	-40.6521	ENID
95.9	4.22	174.4971	-40.2931	ENID
64.7	3.97	176.7318	-39.9777	ENID
33.9	4.46	176.5849	-40.3559	ENID
55.2	3.65	174.4014	-41.2266	ENID
55.0	4.4	174.8334	-41.1380	ENID
52.7	3.59	174.2061	-41.0943	ENID
56.9	4.13	176.6536	-40.1894	ENID
127.6	4.33	177.4357	-37.1126	ENID
62.1	5.94	178.4383	-37.0266	ENID
57.4	4.66	176.4194	-40.2389	ENID
90.3	6.47	174.1805	-41.0523	ENID
45.7	4.07	176.6145	-40.3198	ENID
33.0	5.10	177.9998	-38.6324	ENIS
33.0	4.38	179.2601	-36.8273	ENIS
22.5	3.91	177.3139	-39.6931	ENIS
30.3	3.79	177.3258	-39.5498	ENIS
23.0	4.58	175.4530	-41.5675	ENIS
9.3	4.01	176.9499	-40.3840	ENIS
31.9	4.2	176.0215	-41.6550	ENIS
31.0	3.19	174.5103	-41.1748	ENIS
27.7	3.14	175.6037	-41.5265	ENIS
25.5	4.11	177.7243	-38.9326	ENIS
33.0	3.92	178.0462	-40.4572	ENIS
24.9	3.71	175.7397	-41.3505	ENIS
27.8	3.66	174.8681	-40.1838	ENIS
29.5	3.85	177.2989	-39.2249	ENIS
12.0	3.29	175.7488	-39.5986	ENIS
20.7	4.47	176.5424	-40.4730	ENIS
33.0	4.15	178.0568	-37.2159	ENIS
31.8	4.04	175.4835	-41.0895	ENIS
29.0	3.38	175.6921	-40.6028	ENIS
27.4	3.59	175.5534	-40.6947	ENIS
30.0	3.74	176.1496	-40.5784	ENIS
12.0	3.41	174.8959	-40.1382	ENIS
33.0	4.34	179.4224	-37.6459	ENIS
18.3	4.92	174.9577	-40.1809	ENIS
33.0	4.98	178.9004	-37.1767	ENIS
12.0	4.95	179.1201	-38.3573	ENIS
12.0	4.73	179.4575	-37.6560	ENIS
12.0	5.14	179.2507	-37.7865	ENIS
12.0	4.69	179.3260	-37.8131	ENIS

Appendix 2. Station corrections for the complete data set (four regions) and the non-volcanic data set (three regions).

	Whole data set				Non-volcanic data set		
Station	ENID	ENIS	CVRD	CVRS	ENID	ENIS	CVRD
ARKE	-0.1334	0.0415	0.3401	-0.2044	——	——	——
ASHV	-0.3545	-0.2111	-0.7474	-0.6229	——	——	——
AVNE	-0.1117	0.1111	0.1406	-0.2749	——	——	——
BLTA	0.4431	——	——	——	——	——	——
CAPE	-0.7615	——	——	——	——	——	——
CASM	-0.0612	-0.1014	0.0344	——	-0.2992	-0.2096	-0.3690
CLAM	0.0891	-0.0783	0.0547	——	-0.1531	-0.1700	0.4650
CONM	0.0258	-0.3887	0.4108	——	-0.2230	-0.5351	-0.0214
DKRV	-0.4108	-0.3987	-0.6668	-0.1150	——	——	——
DSZ	0.1133	-0.1086	0.4095	0.9289	-0.2049	-0.3567	-0.4813
EPAV	-0.2757	-0.2639	-0.6967	-0.5604	——	——	——
ERQV	-0.6805	-0.3324	-0.9830	-0.5146	——	——	——
ERRV	-0.1190	-0.1936	-0.5353	-0.3079	——	——	——
FABM	0.5489	0.3653	0.4644	——	0.3142	0.2665	-0.2432
FLAM	-0.0930	——	——	——	-0.3083	——	——
GOHM	0.2315	0.0269	0.5133	——	-0.0121	-0.0859	-0.0578
GRAM	0.4837	0.3362	0.2992	——	0.2418	0.2336	-0.2090
GULV	-0.1222	0.1412	-0.6619	-0.2929	——	——	——
GV2V	-0.1379	0.0343	-0.5804	-0.2057	——	——	——
HRXV	-0.7143	-0.5500	-1.0202	-0.6970	——	——	——
IRVM	-0.0232	-0.1326	-0.0606	——	-0.2639	-0.2292	0.0261
ISIM	-0.0538	-0.1481	-0.0048	——	-0.2879	-0.2565	-0.1396
ISOM	-0.2256	-0.4686	——	——	-0.4649	-0.6261	——
JOPM	0.1084	——	——	——	-0.1266	——	——
KEKM	-0.0451	-0.0956	0.4561	——	-0.2793	-0.2210	0.1633
KENM	0.6775	0.5011	0.5042	——	0.4602	0.3993	0.0872
KHZ	0.1446	0.1008	0.5560	0.4751	-0.1367	-0.0602	-0.0998
KIRG	——	——	——	-0.1568	——	——	——
KOKE	-0.7269	-0.2731	0.0324	-0.1447	——	——	——
KOKM	0.1166	0.0659	0.0941	——	-0.1155	-0.0391	-0.0817
KPSV	-0.2766	-0.0151	-0.5273	0.0901	——	——	——
KUZ	-0.7370	-0.4913	-0.9084	0.0328	——	——	——
LEAM	0.5088	0.3206	0.2499	——	0.2571	0.2227	0.1954
LINM	1.4419	——	——	——	1.2281	——	——
LTZ	0.1010	-0.1408	0.1288	0.6434	-0.1902	-0.3090	0.4520
LYLM	0.2643	0.0262	0.3328	——	0.0122	-0.1135	-0.0929
MAPM	0.0833	0.0041	0.2081	——	-0.1571	-0.0948	0.2134
MARE	-0.2348	-0.0819	0.5828	-0.5090	——	——	——
MNG	0.3307	0.5041	0.8234	0.5120	0.0875	0.3895	0.1374
MOA	0.6532	0.6704	0.9732	0.8625	0.3941	0.5123	-0.0025
MOLM	0.1694	-0.0351	0.0852	——	-0.0799	-0.1232	-0.2266
MOTE	0.0254	-0.2260	0.2539	-0.2456	——	——	——
MOZ	-0.3521	-0.0633	-1.0991	-0.4866	——	——	——
MQZ	1.2019	0.8601	——	——	0.9252	0.7399	——
MRZ	0.2066	0.4726	0.6350	0.4718	0.0521	0.3193	0.2018

	Whole data set				Non-volcanic data set		
Station	ENID	ENIS	CVRD	CVRS	ENID	ENIS	CVRD
MURE	0.4100	0.4222	0.9056	0.3724	——	——	——
NMCM	-0.0673	-0.0987	——	——	-0.3011	-0.1977	——
OHPV	-0.9818	-0.5693	-1.1243	-0.4352	——	——	——
OIZ	-0.1682	-0.0677	-0.4789	0.6451	——	——	——
OKAV	-0.3310	0.0263	-0.3257	0.0163	——	——	——
OKTV	-0.8090	-0.4251	-0.9722	-0.4115	——	——	——
PAKE	-0.3600	-0.4081	0.1882	-0.3944	——	——	——
PARE	0.1878	0.4105	0.8641	0.4895	——	——	——
PKHE	0.1639	-0.0263	0.5017	-0.0108	——	——	——
PKUV	-0.5747	-0.3736	-1.0830	-0.5354	——	——	——
PUHM	0.1651	-0.2083	0.3251	——	-0.0778	-0.3091	0.1960
PUPM	0.5251	0.4549	0.2310	——	0.2879	0.3768	-0.2281
PUZ	-0.1632	0.0860	0.0442	0.1831	-0.4255	-0.1175	0.0044
QRZ	0.2282	0.0644	-0.0227	0.6372	-0.0367	-0.0361	-0.0263
RANE	-0.3589	0.2233	0.1158	-0.4211	——	——	——
REPE	-0.1804	-0.1035	0.4078	-0.3129	——	——	——
RIMM	0.1161	0.1295	0.1352	——	-0.1131	0.0199	0.0366
RUAE	0.2021	0.0934	0.3634	-0.0139	——	——	——
RUNE	-0.6341	-0.5584	-0.3529	-0.5195	——	——	——
SPCM	0.2052	0.1437	——	——	-0.0601	0.0442	——
SRWM	0.1500	0.0070	0.2468	——	-0.0792	-0.1152	0.1315
TAOV	-0.4109	-0.0355	-0.7677	-0.1758	——	——	——
TAUG	——	——	——	0.7750	——	——	——
TEAV	-0.3724	-0.3051	——	——	——	——	——
TEKE	-0.0115	-0.0914	0.3661	-0.3233	——	——	——
TKTH	0.4755	——	——	——	——	——	——
TOAE	-0.1378	-0.1321	0.0222	-0.0236	——	——	——
TOTM	0.7133	0.4448	0.5238	——	0.4763	0.3481	-0.0691
TRLG	——	——	——	0.9504	——	——	——
TTTV	——	——	0.0831	——	——	——	——
TWKH	0.3299	0.3417	0.1726	——	——	——	——
URZ	0.0618	0.0026	0.1311	0.1016	-0.2117	-0.2002	0.1030
VERM	0.6052	——	——	——	0.3916	——	——
WAIM	0.2041	0.0314	0.1538	——	-0.0335	-0.0664	-0.0330
WEL	0.2441	0.7405	0.7747	1.1426	-0.0548	0.4592	-0.0874
WLZ	——	-0.7434	-1.2756	-0.0752	——	——	——
WMAE	-0.0954	-0.0050	0.1809	-0.0569	——	——	——
WNUV	0.1286	0.4279	0.1511	0.5371	——	——	——
WOOE	0.1157	0.4003	0.5817	0.2213	——	——	——
WPOE	-0.2310	-0.3354	0.1145	-0.4862	——	——	——
WRAV	——	0.4003	-0.4242	——	——	——	——
WROM	0.0699	0.2507	0.4325	——	-0.1631	0.1408	0.0556
WTPV	0.1191	0.3189	-0.4143	-0.0293	——	——	——
WVRV	-0.9642	-0.7176	-0.8665	-0.5248	——	——	——
WVZ	0.1129	——	——	——	-0.1649	——	——